Chapter 3
Fabrication Methods of Porous Metals with Directional Pores

Abstract Porous metals with directional pores were investigated from long time ago from the viewpoint to elucidate solidification or casting defects. In 1980s Shapovalov et al. indicated some applicability porous metals with directional pores fabricated through gasar process using high-pressure hydrogen. Then, Nakajima et al. carried out systematic investigations using various casting techniques such as mold casting technique, continuous zone melting technique, and continuous casting technique. The latter is the most superior to control pore size and porosity and is the most suitable for fabricating long-sized casting slabs. To overcome technical difficulty of use of high-pressure hydrogen, very simple fabrication method was invented recently by adding only gas-forming compounds into melt.

Keywords Continuous casting technique • Continuous zone melting technique • Gasar process • High-pressure gas method • Lotus metals • Mold casting technique • Thermal decomposition method

3.1 Historical Background

3.1.1 Ice Wormholes

Chalmers [1] observed porous ice with directional pores called as "ice worms" and discussed the mechanism of the pore formation to the following. Air is a solute that is rejected by water ahead of the freezing process during the solidification of water. It accumulates in the advancing interface until its concentration is high enough for bubbles to nucleate. Once a bubble has formed, it grows because air diffuses into it. If the interface continues to move forward, the bubble cannot grow laterally, and so, it grows forward to form the cylindrical bubble sometimes known as an ice worm as shown in Fig. 3.1. Close inspection shows that ice worms never start at the surface of the ice, but always a little way in; this is because some freezing must

DOI 10.1007/978-4-431-54017-5_3, © Springer Japan 2013

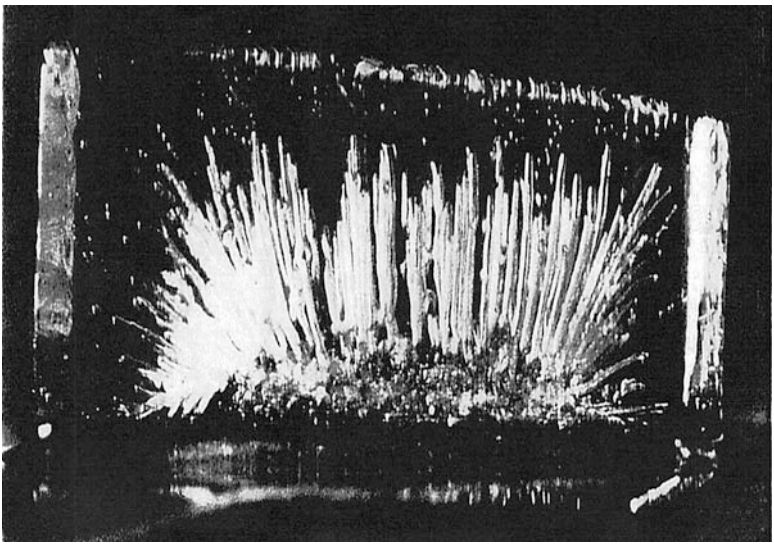

Fig. 3.1 Ice worms form during the growth of an ice cube because the ice crystal (grew from the bottom) rejects air that was dissolved in the water (Reprinted with permission from [1] © 1959 Scientific American, Inc.)

occur before the air accumulating at the interface reaches sufficient concentration to cause the nucleation of a bubble. Here again growth occurs more easily than the nucleation that starts it.

The ice worms that grow in ice cubes frequently look like strings of pearls. This reflects the fluctuation in the freezing rate due to the intermittent operation of the refrigerator. When freezing is slow, more air diffuses into the bubbles and they grow larger; during periods of fast growth, there is less times for diffusion and the bubble decreases in cross section. Fast freezing suppresses the formation of ice worms. Because insufficient air diffuses into the bubbles to permit them to grow, the ice contains a large number of very small, round bubbles. On the other hand, very slow freezing permits the rejected air to diffuse away from the interface; because the concentration of air never reaches the nucleation point, neither bubbles nor ice worms appear. Ice grown in flowing water is also usually free of bubbles and ice worms; the continuous removal of the water prevents the buildup of a high concentration of dissolved air, hence the absence of bubbles in the ice cubes produced by some commercial freezers.

For freezing to take place continuously, the heat of fusion must somehow be carried away from the region where ice is forming. Normally, as in the growth of ice cubes or of ice on the surface of a lake, the heat is extracted by conduction through the ice that has already formed. The water–ice interface tends to remain flat, because any region of convex curvature is cooled less efficiently than the remainder, and its rate of freezing is retarded until a smooth interface is restored. However, if the ice crystal is growing in supercooled water, its growth takes an entirely

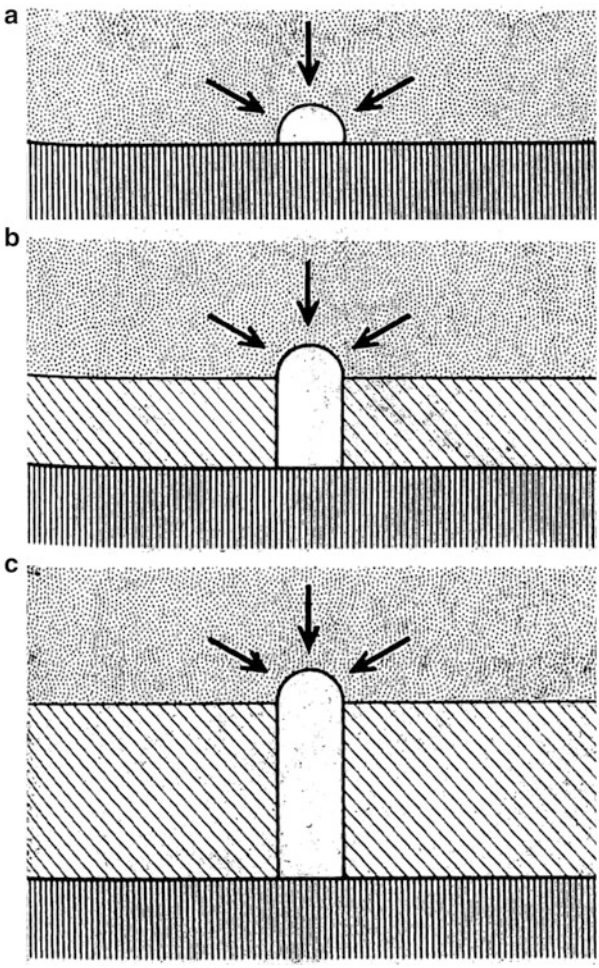

Fig. 3.2 Growth of ice worm. Diagonal hatching shows accrual of ice; the *arrows*, dissolved air diffusing in to worm. (**a**) A pore nucleates in water in vicinity of ice. (**b**) As the interface between ice and water proceeds upward, enriched air which is rejected in the ice diffuses into the pore. (**c**) An elongated-cylindrical pore continues to grow in the direction of movement of the interface. (Reprinted with permission from [1] © 1959 Scientific American, Inc.)

different form. Because the latent heat of fusion flows outward into the supercooled liquid, cooling is more efficient at a convex region; convex regions therefore become even more convex. The latent heat produced by the growth of a convexity suppresses growth in the vicinity, and so a projection becomes an isolated spike as illustrated in Fig. 3.2. The direction in which such branching or "dendritic" growth may go in various substances depends on the characteristic molecular arrangement of the crystal. In the case of ice, the spike may grow in any one of six directions. Once a spike has formed, the supercooled environment may permit the growth of lateral secondary, ternary, and even quaternary branching spikes, always in the proper crystallographic directions. This explanation is highly suggestive to investigate the following porous metal science.

3.1.2 Porous Metals with Directional Pores

Recently, a new type of porous metals whose long-cylindrical pores are aligned in one direction has been fabricated by unidirectional solidification under a pressurized hydrogen, nitrogen, or oxygen gas. Many gas pores are evolved from insoluble hydrogen (nitrogen or oxygen) in solids while hydrogen (nitrogen or oxygen) dissolves significantly in liquids. Formation of elongated gas pores during solidification has been investigated by Imabayashi et al. [2], by Svensson and Fredriksson [3], and by Knacke et al. [4]. Furthermore, Shapovalov et al. [5] fabricated longer cylindrical pores by adopting a unidirectional solidification technique at a high pressure of hydrogen. Nakajima et al. [6, 7] also produced porous iron, copper, magnesium, nickel, and those alloys in high-pressure hydrogen or nitrogen atmosphere and porous silver in high-pressure oxygen by means of the Czochralski method and a unidirectional solidification method. The processing technique is different from that of cellular and foamed metals, since it allows a control of pore size, pore direction, and overall porosity. High-pressure hydrogen or other gas is filled in the pores of the porous metals during an invariant reaction of the so-called gas-evolution crystallization reaction, where the melt is solidified to transform into a solid solution and a gas phase [8]. During solidification, the gas is rejected from the solid metal at the solid–liquid interface and forms long pores that are aligned parallel to the solidification direction. Shapovalov et al. named this method as gasar, which means a Ukrainian acronym for gas-reinforced composite metals [9]. However, it turns out by the systematic investigations by Nakajima et al. that gas pores do not affect to reinforce the porous metals. Therefore, a term from their shape is considered to be more suitable for the name of the porous metals. Nakajima group called their materials as “lotus-type porous metals” (hereafter we call lotus metals) because the morphology of the material resembles that of a lotus root. The strength of lotus metals is superior to that of conventional porous metals such as cellular and foamed metals [7, 10].

Thus, such lotus and gasar metals are expected as a new category of engineering materials.

3.2 High-Pressure Gas Method (PGM)

3.2.1 Mold Casting Technique

As mentioned above, the gas pores are evolved by insoluble gas atoms in the solid when the melt dissolving gas is solidified because of the gas solubility difference between liquid and solid. Figure 3.3 shows the temperature dependence of hydrogen solubility in both states of various metals [11]. The solubility of hydrogen increases with increasing temperature in both solid and liquid. For the metals in which a discontinuous abrupt decrease is observed in the solubility at the melting

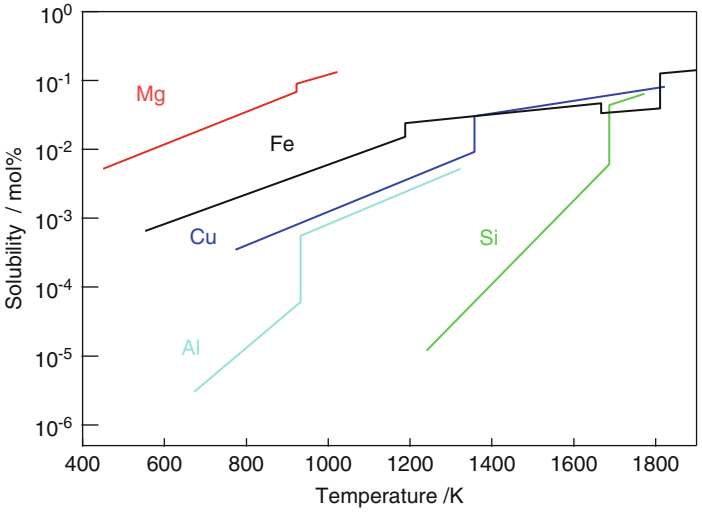

Fig. 3.3 Temperature dependence of hydrogen solubility in solids and liquids of various metals under the hydrogen pressure of 0.1 MPa [11]

point when the temperature is lowered, significant pore evolution occurs in the solidified metals so that the lotus and gasar structure can be easily fabricated during the unidirectional solidification.

So far, casting method is usually adopted as the fabrication technique of the lotus and gasar metals. The peculiar difference of lotus and gasar metals from the cellular and foamed metals is the pore morphology; while the former has elongated cylindrical pores aligned in the solidification direction, the latter has always almost spherical pores distributed randomly in the matrix. Figure 3.4a shows schematic drawing of the mold casting technique to fabricate lotus and gasar metals; a metal inside a crucible is melted by an induction heating in a high-pressure gas atmosphere. The gas is dissolved up to the equilibrium gas concentration into the molten metal under a given gas pressure according to the Sieverts law [12]. The melt saturated with gas is poured into the mold. When some part of the mold is cooled down by a chiller or circulated water, the melt can be solidified unidirectionally from the vicinity of the cooling part. Figure 3.4b shows the overviews of the fabrication apparatus of mold casting technique installed at Nakajima Laboratory of Osaka University. The elongated pores can evolve and grow by the influence of the unidirectional solidification. The pore growth direction can be controlled by changing the location of the cooling part (chiller). Figure 3.5 illustrates three different types of the molds. When the bottom of the mold is water-cooled, the molten metal is unidirectionally solidified upwards from the bottom part so that the directional pores grow in the upward direction. When the lateral side of the mold is cooled down, the solidification takes place inwardly from the surrounding, and thus, the pore distribution becomes radial. If a particular cooling part is not set up in the

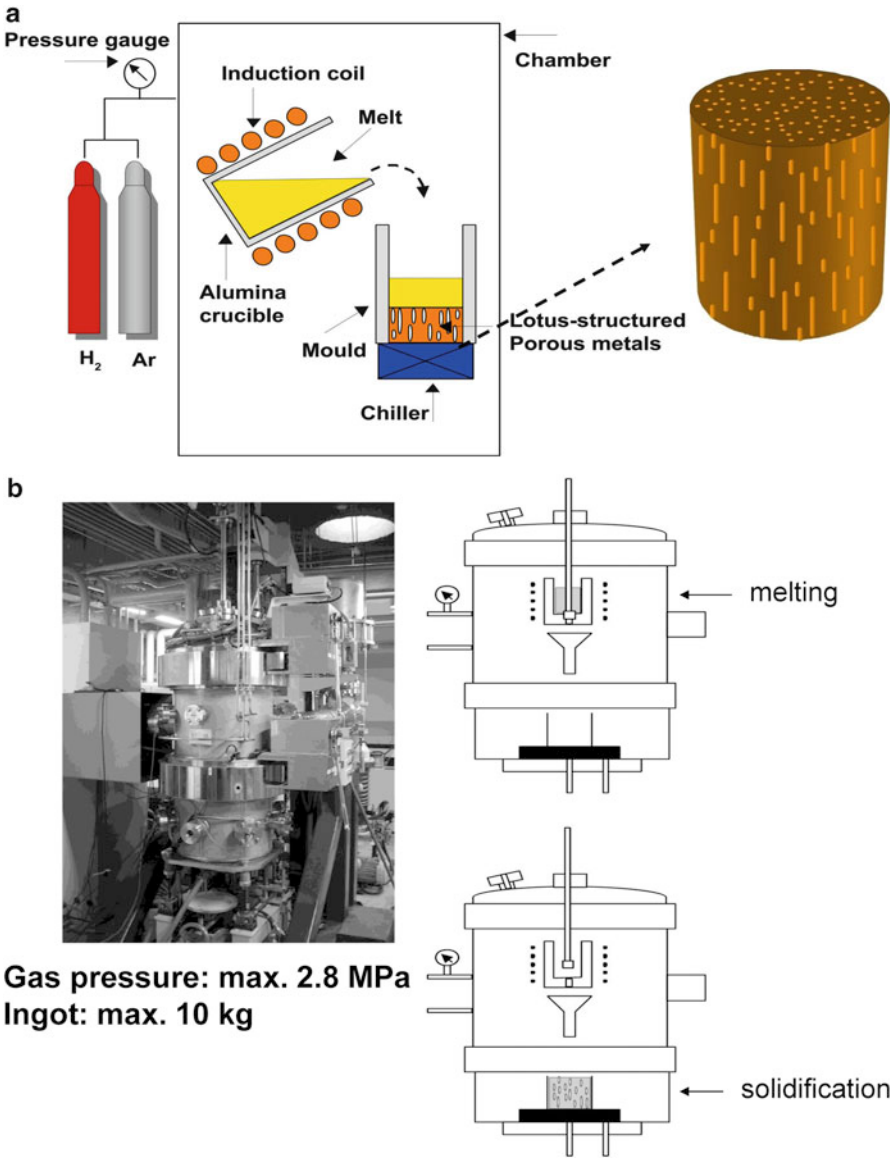

Fig. 3.4 (**a**) Schematic drawing of principle for fabrication of lotus metals through mold casting technique (Reprinted with permission from literature of Prog Mater Sci 52(2007) 1091–1173, ©2006 Elsevier Ltd). (**b**) Overview of the apparatus for fabrication of lotus metals through mold casting technique installed at Nakajima Laboratory of Osaka University. The *right-hand upper figure* shows that the metal is melted by the crucible by heating radio-frequency induction coil. The *right-hand lower figure* shows that after the stopper rod is lifted to open the bottom hole of the crucible, the melt is dropped down through a funnel into the hearth whose bottom is cooled by a chiller. Unidirectional solidification takes place to produce the lotus metals

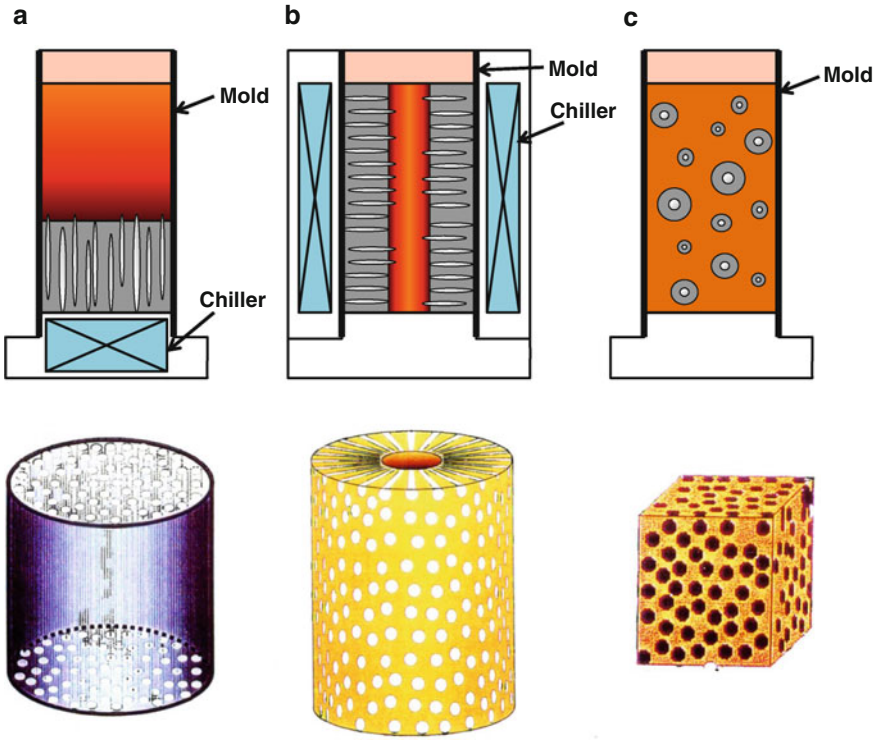

Fig. 3.5 Three different types of molds for casting and resulting pore configurations in the porous metals: (**a**) unidirectional pores, (**b**) radial pores, and (**c**) isolated spherical pores. (**a**) and (**b**) are anisotropic pores, while (**c**) is isotropic pores (Reprinted with permission from literature of Prog Mater Sci 52(2007) 1091–1173, © 2006 Elsevier Ltd)

mold, the spherical pores start to grow everywhere and distributed randomly whose morphology resembles pumice stones.

In general, the porous, cellular, and foamed metals are characterized by pore growth direction, pore size, and porosity. As mentioned earlier, while the pore direction, pore size, and porosity of the cellular and foamed metals are not easy to control by the fabrication methods, those of the lotus and gasar metals are relatively easier by those fabrication methods because the direction of the solidification, gas pressure, gas content, and the solidification velocity can be controlled. The parameters to control the pore morphology can be listed up as

the melt temperature
the solidification rate
the temperature gradient of the interfacial region of liquid–solid phase
the dissolving gas pressure during melting and solidification
the inert gas pressure during melting and solidification

Table 3.1 Lotus metals to be fabricated and available gases

Available gas	Lotus metals to be fabricated
Hydrogen	Iron, carbon steel, stainless steel, aluminum, magnesium, nickel, copper, cobalt, tungsten, manganese, chromium, beryllium, and those alloys
Nitrogen	Iron, carbon steel, stainless steel
Oxygen	Silver

The lotus metals to be fabricated and available gases are compiled in Table 3.1. Hydrogen gas is used to fabricate various lotus metals and alloys: iron, nickel, aluminum, copper, magnesium, cobalt, tungsten, manganese, chromium, beryllium, and those alloys. Fortunately, most of the base metals for commercially available practical alloys can be made porous. However, there are some problems; as the hydrogen concentration dissolving in molten aluminum is small, the porosity of lotus aluminum is less than 40 % by the present technique. On the other hand, although fabrication of porous titanium is possible, the pore shape is not cylindrical, but spherical, because of high dissolving concentration of hydrogen.

Since hydrogen is inflammable and explosive when oxygen is present, its use is not convenient from the industrial point of view. Use of other gases than hydrogen is desirable. It is well known that nitrogen is an important alloying element widely used to improve corrosion resistance and mechanical properties of steels. The temperature dependence of nitrogen solubility in solid and liquid of iron is similar to that of hydrogen, which exhibits a large nitrogen solubility difference between solid and liquid of iron at the melting temperature [13–15]. Moreover, it is known that an invariant reaction [8] of "gas-evolution crystallization reaction" takes place in the Fe-N system, in which the iron melt dissolving nitrogen is solidified to transform into a primary solid solution and nitrogen gas. Utilizing the nitrogen solubility difference between liquid and solid, lotus iron was fabricated by the abovementioned technique [16]. Using oxygen gas, porous silver can be produced, because metallic oxide of silver cannot be formed in oxygen atmosphere when the molten silver is solidified [17].

Figure 3.6 shows typical examples of optical micrographs on the cross section (above) and the longitudinal sections (below) of lotus copper.

3.2.2 Continuous Zone Melting Technique

The mold casting technique was usually used to produce lotus-type porous metals. For a few porous metals such as copper [6, 7] and magnesium [18] as shown in Fig. 3.6, long-cylindrical pores were grown in the same direction as the unidirectional solidification. The pore size in the section perpendicular to the solidification direction depends on the solidification velocity; the higher the solidification velocity, the smaller the pore size [19]. Since these metals exhibit high-thermal

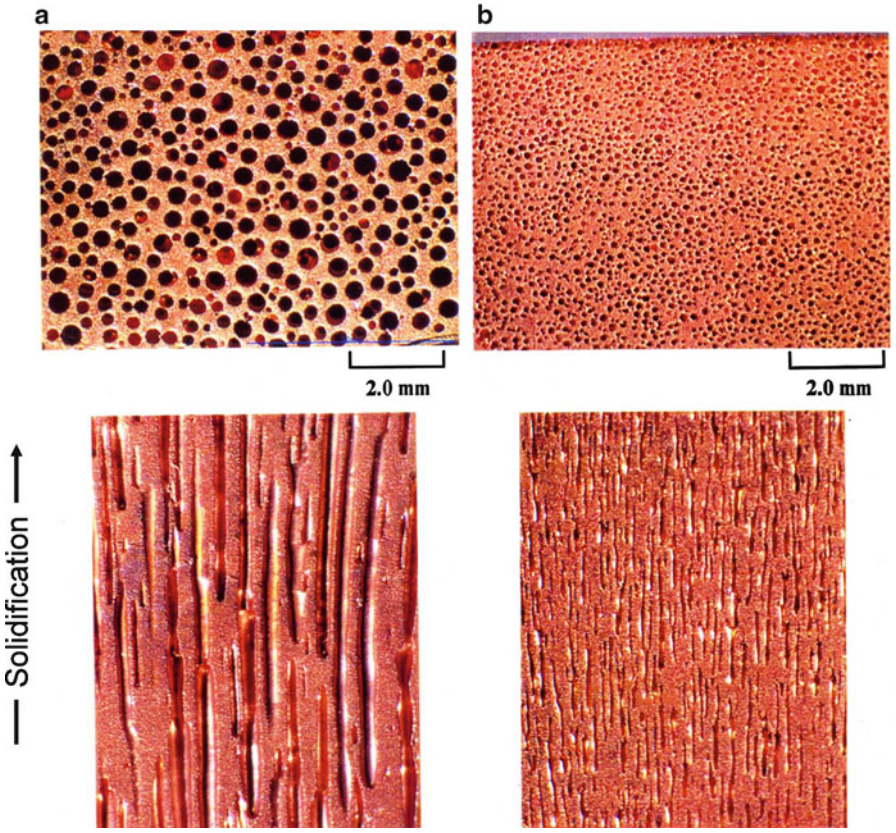

Fig. 3.6 Typical examples of optical micrographs on the cross sections of lotus-type porous copper fabricated through mold casting technique at different hydrogen pressure. The above is the cross sections perpendicular to the solidification and the below is the cross sections parallel to the solidification. (**a**) 0.4 MPa hydrogen pressure, porosity 44.9 %, and (**b**) 0.8 MPa hydrogen pressure, porosity 36.6 % (Reprinted with permission from literature of Prog Mater Sci 52 (2007) 1091–1173, © 2006 Elsevier Ltd)

conductivity, the solidification proceeds with almost constant solidification rate through the whole of ingot. Thus, porous metals with uniform pore size and porosity can be produced by this technique as shown in Fig. 3.6. However, the same technique cannot be applied to fabricate porous metals and alloys with low-thermal conductivity such as stainless steel [20]. For the metals and alloys with low-thermal conductivity, although the heat from the melt is easily dissipated to the water-cooled plate during the solidification process, the cooling becomes slower at the upper part of the solidified ingot where it is far from the cooling part and thus the pores become coarse. As a result only porous metals and alloys with nonuniform pore size and porosity can be produced as illustrated in Fig. 3.7. In order

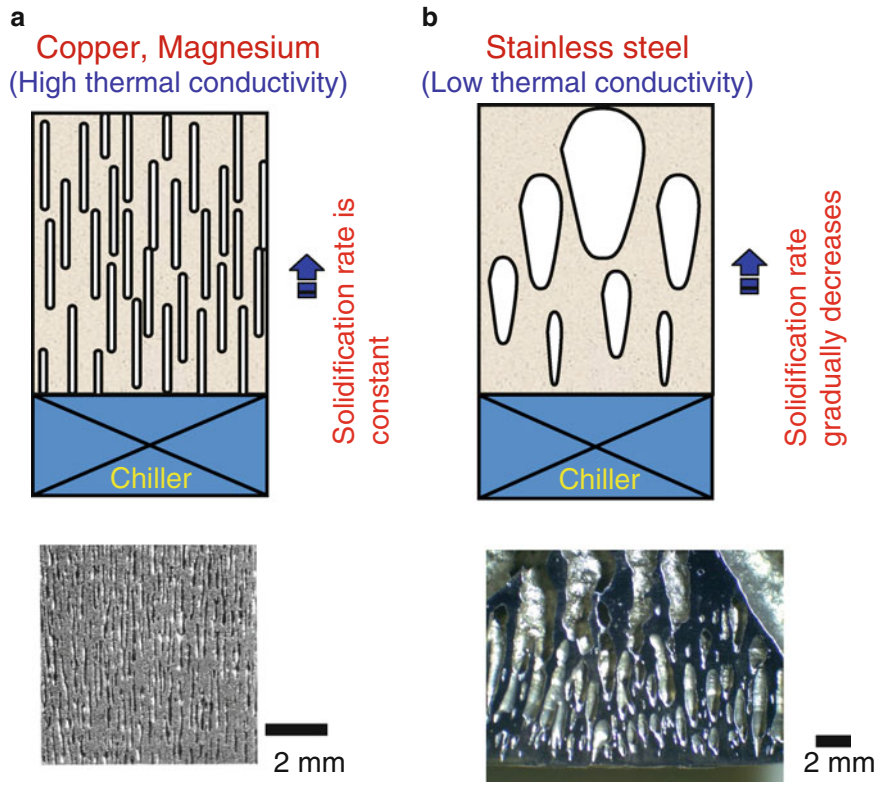

Fig. 3.7 Comparison of the evolution of pores in porous metals fabricated by mold casting technique in gas atmosphere. The *above* is schematic drawings of pore evolution during the unidirectional solidification. The *below* is optical micrographs of the sectional views perpendicular to the solidification. The *left* is lotus copper, and the *right* is stainless steel. (**a**) The uniform pore size and porosity are observed in copper and magnesium with high thermal conductivity, and (**b**) various pore size and porosity are found in stainless steel with low-thermal conductivity. The magnitude of the thermal conductivity affects the solidification velocity of the melt (Reprinted with permission from literature of Prog Mater Sci 52(2007) 1091–1173, © 2006 Elsevier Ltd)

to overcome the shortcoming, a novel technique was invented by the present author to fabricate pore-elongated lotus metals and alloys even with low-thermal conductivity [21, 22]. Figure 3.8 illustrates the schematic setup of the continuous zone melting technique, which consists of radio-frequency induction coil, blowers, specimen rod, and movable specimen holders; the induction coil is used for the zone (restricted area) melting of the rod-shaped specimen, while the blower is helpful for further cooling of the melt metal. These components are placed into a high-pressure chamber filled with gases such as hydrogen (or nitrogen) and argon. While a part of the specimen rod is melted by induction heating, the hydrogen (or nitrogen) gas is absorbed into the melt up to the gas equilibrium solubility in the pressurized gas atmosphere according to Sieverts' law. Concurrently, the specimen

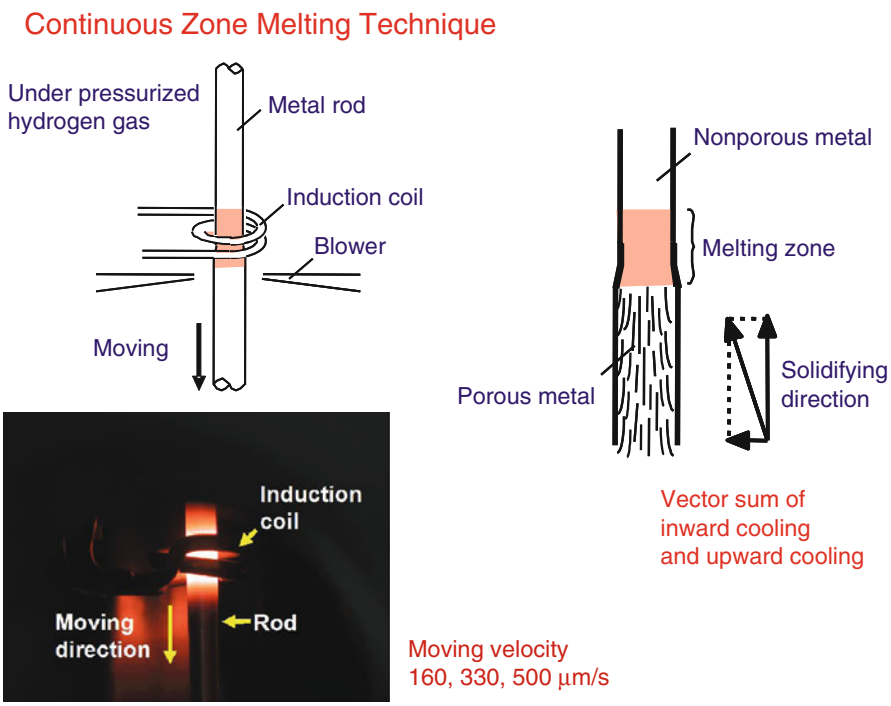

Fig. 3.8 Schematic drawings and a photograph of the overview for the melting part of continuous zone melting technique. After passing the melting zone, the rod in the lower part is expanded to form lotus metals (Reprinted with permission from literature of Prog Mater Sci 52(2007) 1091–1173, © 2006 Elsevier Ltd)

rod is moved downward at a given transfer velocity. In the lower part of the melt zone, the solidification takes place simultaneously. Then, directional elongated pores are evolved by precipitation of insoluble gas of hydrogen (or nitrogen) in the solidified specimen rod. If the transfer velocity is kept constant, the solidification velocity becomes constant so that the pore size should be constant. The direction of the growing pores is determined by the vector sum of two kinds of solidification directions: an inner cooling vector and an upward cooling vector as shown in the same figure. It is noticed after observation of the sectional view of the specimen that the upward cooling is usually dominant in the interior part of the rod, while the inner cooling effect cannot be ignored near the surface region of the specimen rod. The stainless steel (e.g., SUS304L) exhibits a low-thermal conductivity so that porous stainless steel with homogeneous pore size and porosity is impossible by the conventional mold casting technique as shown in Fig. 3.7. However, lotus stainless steel with homogeneous pore size and porosity is successfully fabricated by so-called continuous zone melting technique. This technique has an advantage that we can control the solidification velocity by changing the

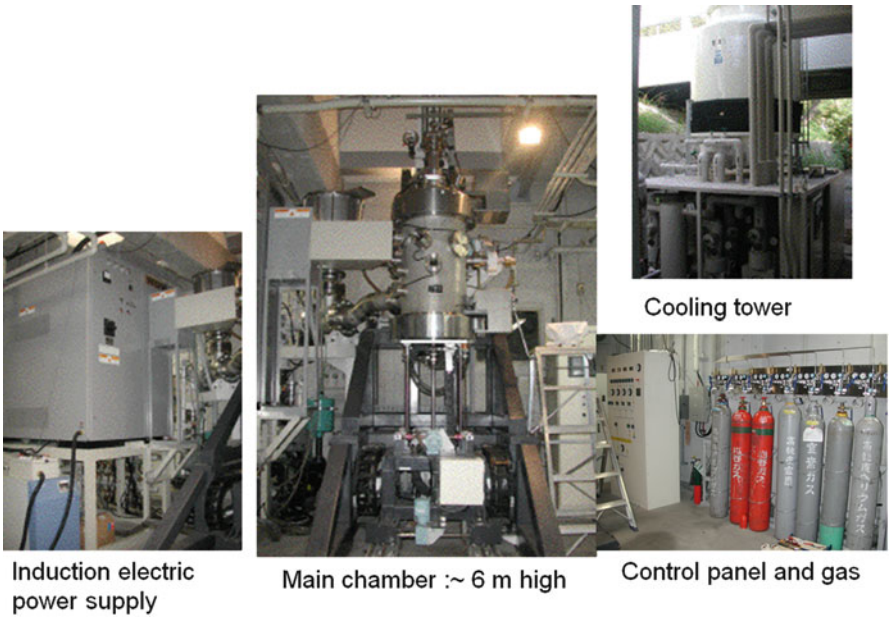

Fig. 3.9 Overview of the fabrication apparatus of lotus metals through continuous zone melting technique installed at Nakajima Laboratory of Osaka University

lowering speed of the specimen rod regardless of the magnitude of thermal conductivity [23]. On the other hand, the solidification velocity is not controllable to a wide range by the conventional mold casting technique and is almost uniquely determined by its own inherent thermal conductivity. Figure 3.9 shows the photographs of the overview of the fabrication apparatus for continuous zone melting technique. Figure 3.10 shows a sectional view of a lotus stainless steel rod (SUS304L) and the pore size and the porosity are almost identical everywhere through the solidified specimen rod more than 300 mm in length. The length of the lotus metals and alloys to be fabricated by the continuous zone melting technique is essentially endless, but in the present chamber, the movable height is limited to less than 300 mm. This continuous zone melting technique is a promising technique in order to produce long-sized lotus rods for commercial application.

3.2.3 Continuous Casting Technique

The continuous casting technique is extensively used as a mass-production method for ferrous and nonferrous metals and alloys. In this conventional continuous casting process, the solidified ingot can pass through the mold smoothly due to the solidification shrinkage from the melt. However, for fabrication process of lotus

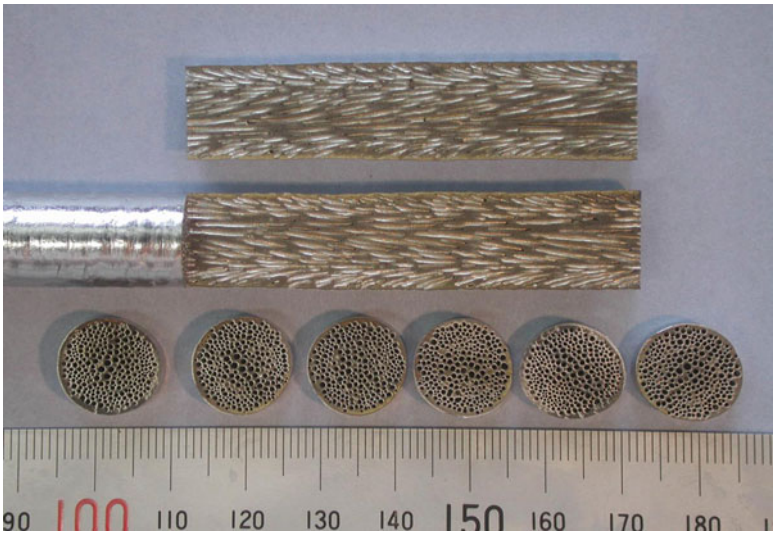

Fig. 3.10 Sectional views of lotus stainless steel fabricated by continuous zone melting technique in the 2.0 MPa hydrogen atmosphere. The transfer velocity of the rod is 330 μm s^{-1}. Resulting porosity and average pore size are 40 % and 320 μm, respectively, both of which are almost uniform in the whole part of the ingot (Reprinted with permission from literature of Prog Mater Sci 52(2007) 1091–1173, © 2006 Elsevier Ltd)

metals, a large volume expansion due to large amount of pore formation occurs when the solidified ingot is passed through the mold. It was initially thought that such an expansion would present problems with the stacking of the ingot in the mold and that consequently this technique could not be applied to the fabrication of lotus metals. However, it was later realized that such a large expansion inherent from the pore evolution was released to push the volume toward the copper part of the molten metal, so that the melt can accommodate the large strain of the solidified ingot. That is why the continuous casting technique is applicable to the fabrication of lotus metals.

Through this technique, the solidification velocity can be controlled by the transfer velocity in hydrogen gas atmosphere. Since the pore morphology of lotus metal is related to the solidification velocity, it is suggested that the pore morphology of lotus metals can be easily controlled by the technique. Park et al. successfully fabricated long-sized lotus copper by controlling its pore size and porosity [24].

Slabs of lotus copper were fabricated by a vacuum-assisted and pressurized continuous casting apparatus, as illustrated in Fig. 3.11. The apparatus consists of a crucible with a rectangular hole at the bottom, a dummy bar for preventing the melt from flowing through the hole, and induction heating coil, and a mold which is surrounded by a water-cooled chill block and pinch rollers to control the transfer velocity of the dummy bar. The solidified ingot bar (slab) can be produced to 700 mm long. Pure copper was melted in the crucible by radio-frequency induction

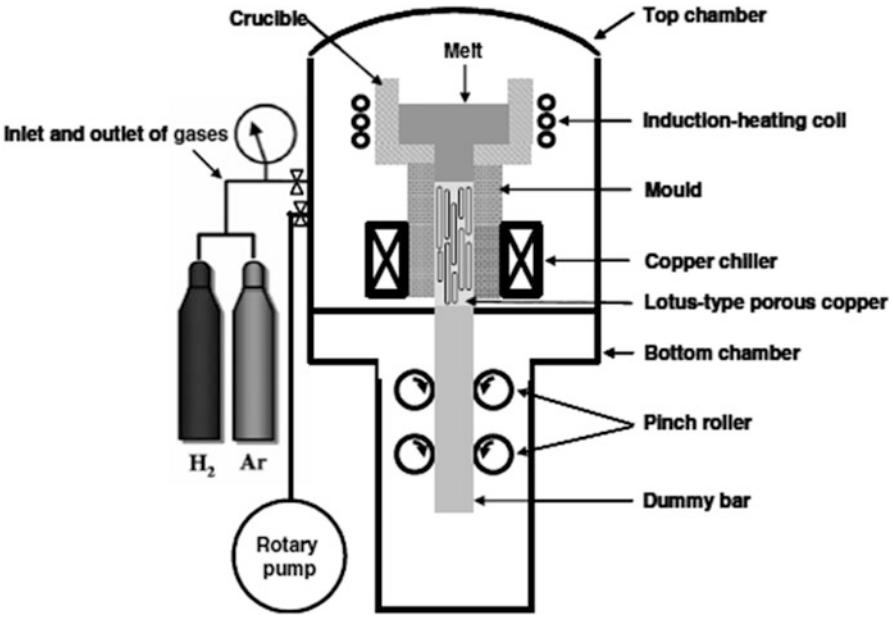

Fig. 3.11 Schematic drawing of continuous casting apparatus (Reprinted with permission from [24]. © 2007 Acta Materialia Inc.)

heating under a hydrogen gas pressure of 2.0 MPa. The temperature of the molten copper in the crucible was monitored by a W-5Re/W-26Re thermocouple, which was available in the hydrogen atmosphere and was set to be 1,573 K. The melt was pulled down by the dummy bar of nonporous copper through the cooled mold at a given transfer velocity. By the cooling of the melt through both the mold and the connected dummy copper bar, the melt was simultaneously and continuously solidified. Then, the hydrogen in the melt was rejected at the solid–liquid interface due to the solubility gap of hydrogen between liquid and solid, and cylindrical pores aligned parallel to the solidification direction were formed. Figure 3.12 shows the photographs of the overview of fabrication apparatus for continuous casting technique installed at Nakajima Laboratory of Osaka University.

Figure 3.13a, b shows outer view and cross-sectional view of lotus copper rod fabricated in the mixture gas of hydrogen 0.25 MPa and argon 0.15 MPa under transfer velocity of 100 mm min^{-1}, respectively. The pore size and porosity are almost identical everywhere through the solidified specimen plate more than 700 mm. The length of the fabricated lotus metals should be essentially endless, but in this chamber, there is some size limitation; the movable height was limited to less than 1,000 mm. Figure 3.14 shows the cross-sectional views of the lotus copper fabricated at various transfer velocities under various hydrogen gas pressure; these views are parallel and perpendicular to the transfer direction. In the observed cross

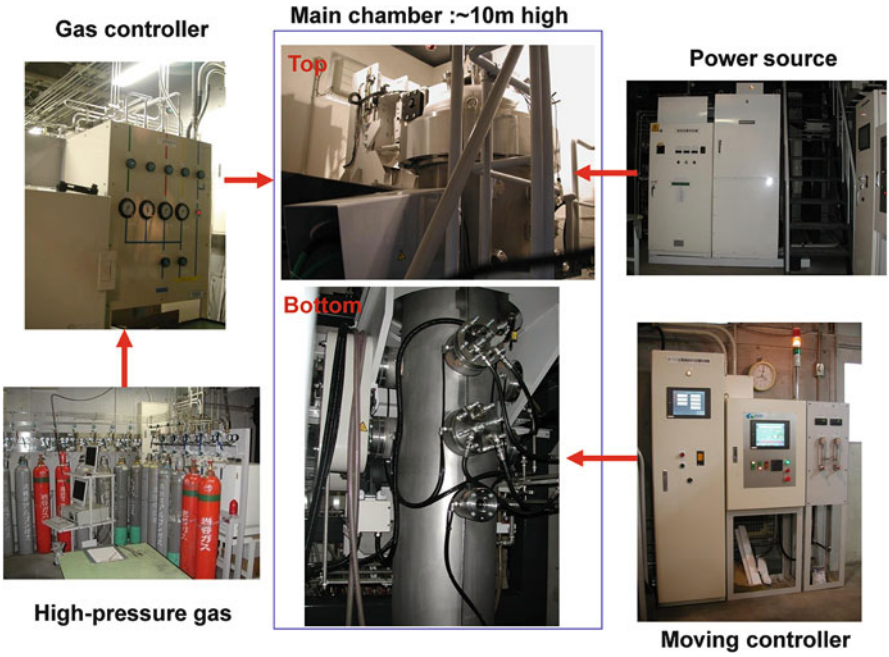

Fig. 3.12 Photographs of the overview of fabrication apparatus for the continuous casting technique installed at Nakajima Laboratory of Osaka University. The *central upper photo* shows the upper chamber set up by heating part and solidification part, while the *central lower photo* shows lower chamber set up by mechanical pinch roller to pull down the ingot slab

section of the slabs fabricated at 1 mm min^{-1} under 1.0 or 2.0 MPa hydrogen. Three large (diameter $\geq$ 5 mm) and many small pores are distributed inhomogeneously; many small pores are also found in the interior of the large pores. The shapes of the pores are irregular. Thus, it is considered that the large pores are found by the cohesion of a few small pores; the volume of the small pores increases during solidification when the amount of hydrogen diffused from the solid to the pores increases with decreasing transfer velocity. However, the slabs fabricated at a high-transfer velocity possess long-cylindrical pores distributed homogeneously. The pore size decreases and the number density of the pores increases with an increase in not only the transfer velocity but also the hydrogen gas pressure.

Figure 3.15 shows the relationship between the porosity and the transfer velocity under hydrogen gas pressures of 1.0 and 2.0 MPa. The porosity decreases with increasing hydrogen gas pressure, while the porosity is almost constant and independent of the transfer velocity. Such a tendency is consistent with the results reported by Hyun and Nakajima [19] and Ikeda et al. [23]; they respectively fabricated lotus copper and stainless steel using the mold casting and continuous zone melting techniques at various solidification velocities under various gas pressure. Figure 3.16 shows the effect of transfer velocity on the average pore

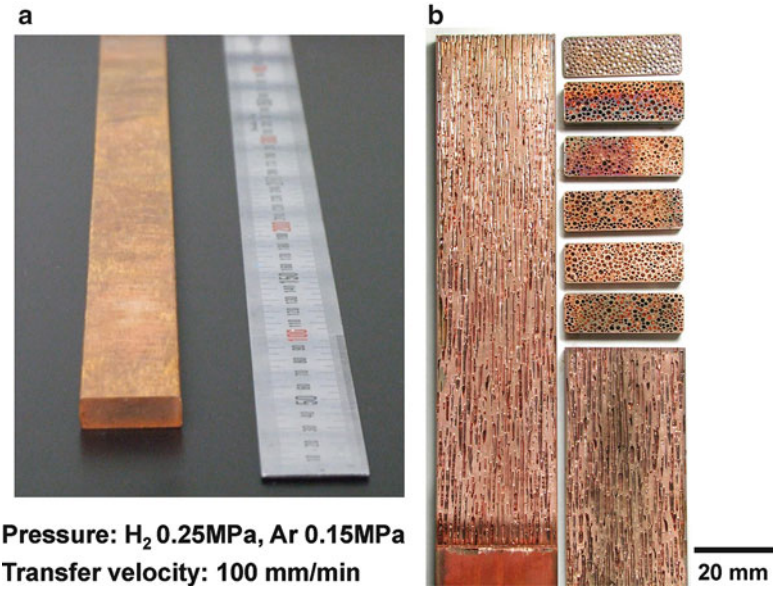

Fig. 3.13 (**a**) A photograph of the overview of lotus copper fabricated using the continuous casting technique and (**b**) cross sections parallel and perpendicular to the transfer direction of the lotus copper fabricated in mixture gases of hydrogen 0.25 MPa and argon 0.15 MPa by continuous casting technique (Reprinted with permission from literature of Prog Mater Sci 52(2007) 1091-1173, © 2006 Elsevier Ltd)

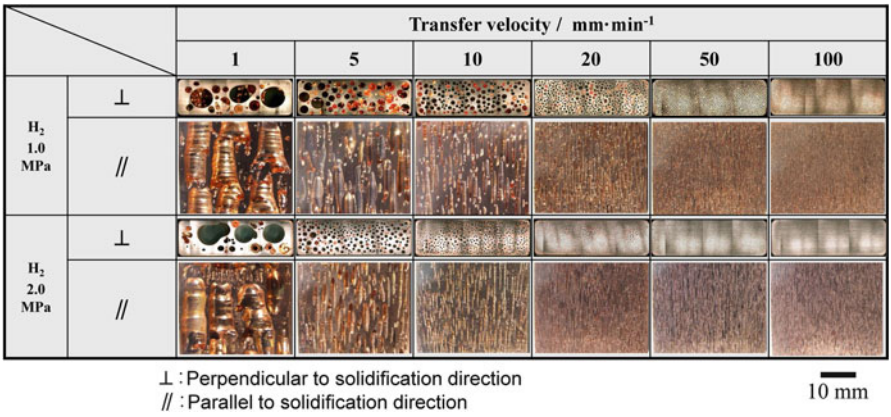

Fig. 3.14 Cross sections perpendicular and parallel to the transfer direction of lotus copper fabricated at various transfer velocities under hydrogen gas pressure of 1.0 and 2.0 MPa (Reprinted with permission from [24]. © 2007 Acta Materialia Inc.)

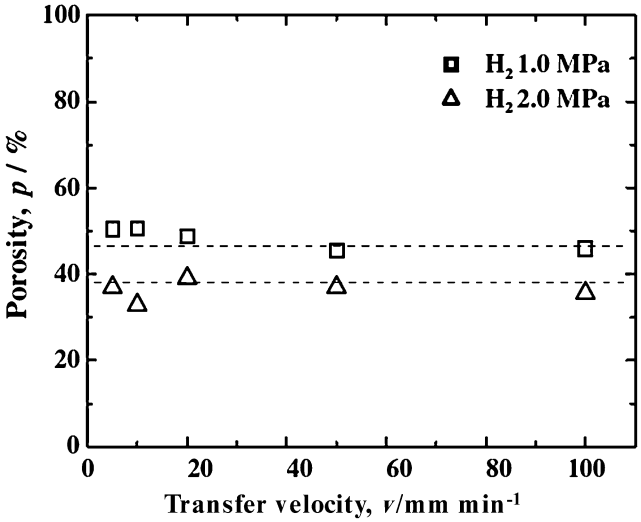

Fig. 3.15 Porosity against the transfer velocity of lotus copper fabricated under hydrogen gas pressure of 1.0 and 2.0 MPa (Reprinted with permission from [24]. © 2007 Acta Materialia Inc.)

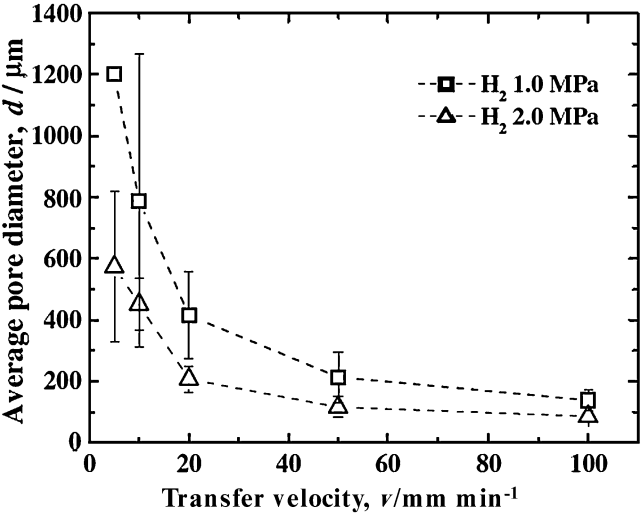

Fig. 3.16 Average pore diameter against the transfer velocity of the lotus copper fabricated under hydrogen gas pressure of 1.0 and 2.0 MPa (Reprinted with permission from [24]. © 2007 Acta Materialia Inc.)

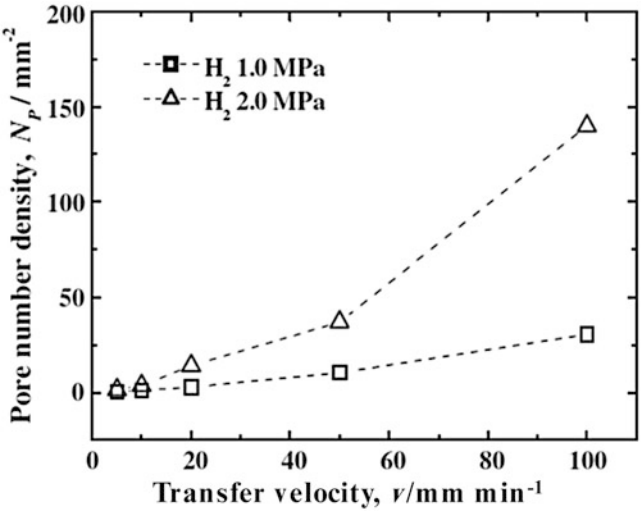

Fig. 3.17 Pore number density calculated using the average pore diameter and the porosity in a unit area (1.0 × 1.0 mm^2) on a cross section perpendicular to the transfer direction at various transfer velocities under hydrogen gas pressure of 1.0 and 2.0 MPa (Reprinted with permission from [24]. © 2007 Acta Materialia Inc.)

diameter d under each hydrogen gas pressure. The average pore diameter decreases with an increase in not only hydrogen gas pressure but also the transfer velocity. In addition, the density of the pore number increases with increasing transfer velocity as shown in Fig. 3.14. Figure 3.17 shows the change of the pore number density N_p calculated using the average pore diameter and the porosity in a cross-sectional area of 1.0 × 1.0 mm^2, with the transfer velocity. The pore number density increases with increasing transfer velocity, while an increase in hydrogen gas pressure brings about an increase in the pore number density for a given transfer velocity. These indicate that the pore number density is affected not only by the transfer velocity but also by the total gas pressure. The pore length l was also affected by the transfer velocity as shown in Fig. 3.18, which decreases with increasing transfer velocity.

The pore growth direction is affected by the transfer velocity. Figure 3.19 shows the angle θ between the pore growth direction and the transfer direction in various positions of the slab in a direction perpendicular to transfer direction. In the center of the slab, the angle is almost zero and independent of the transfer velocity. On the other hand, the pore growth angle increases when the position of the slab moves from center to near the surface, and the pore growth angle increases more with increasing transfer velocity. Thus, the pore growth angle is affected by the transfer velocity, and the effect increases with increasing transfer velocity. Figure 3.20 shows the magnifications and the schematics of the pore formation position near the surface. The thickness t decreases with increasing transfer velocity as shown in Fig. 3.21.

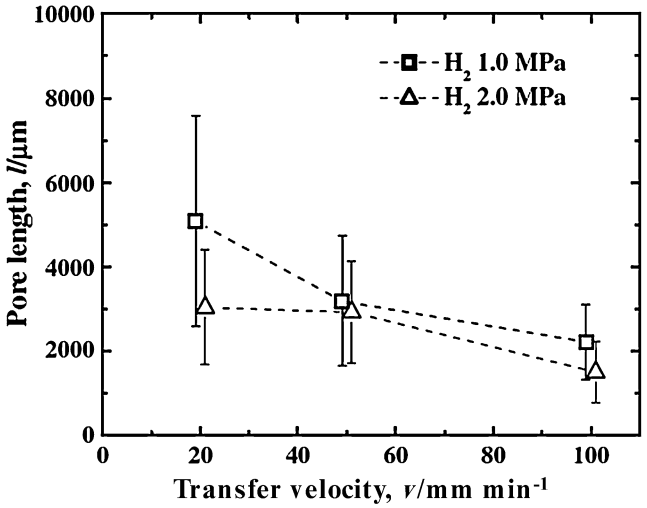

Fig. 3.18 Pore length against the transfer velocity of lotus copper fabricated under hydrogen gas pressure of 1.0 and 2.0 MPa (Reprinted with permission from [24]. © 2007 Acta Materialia Inc.)

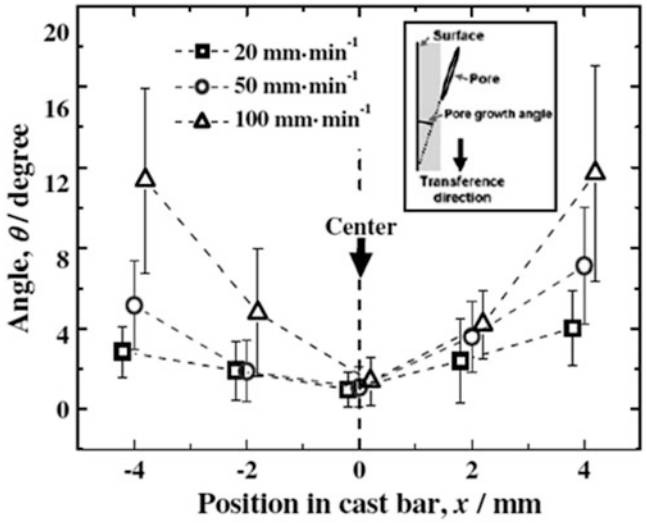

Fig. 3.19 Angle between the pore growth direction and the transfer direction in various positions of the slab in a direction perpendicular to the transfer direction; the slab was fabricated at various transfer velocities under a hydrogen gas pressure of 1.0 MPa (Reprinted with permission from [24]. © 2007 Acta Materialia Inc.)

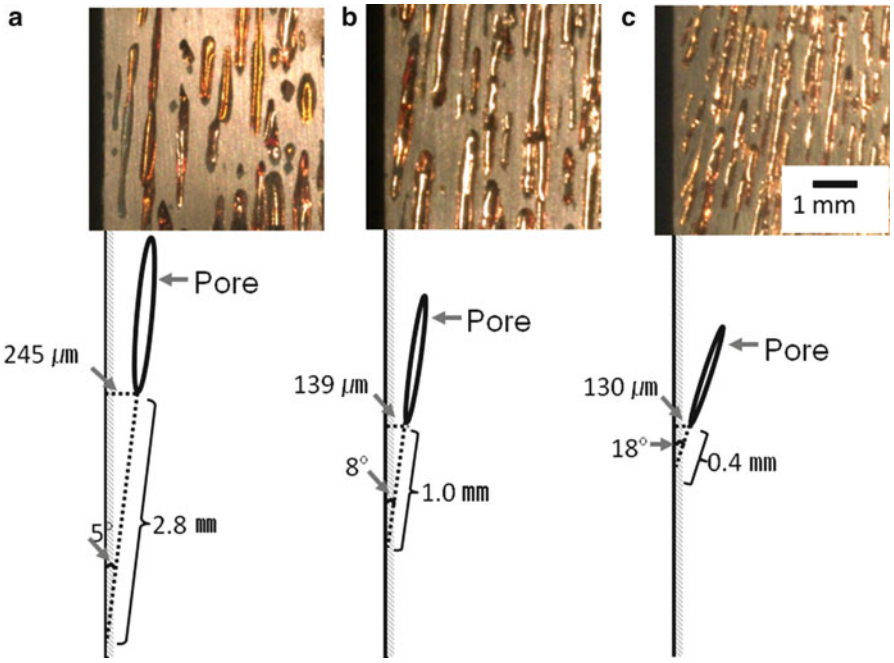

Fig. 3.20 Photographs (*upper row*) and schematic (*lower row*) of the pore formation position near the surface fabricated by the continuous casting technique at the transfer velocity of (**a**) 20 mm min^{-1}, (**b**) 50 mm min^{-1}, and (**c**) 100 mm min^{-1} under a hydrogen pressure of 1.0 MPa (Reprinted with permission from [24]. © 2007 Acta Materialia Inc.)

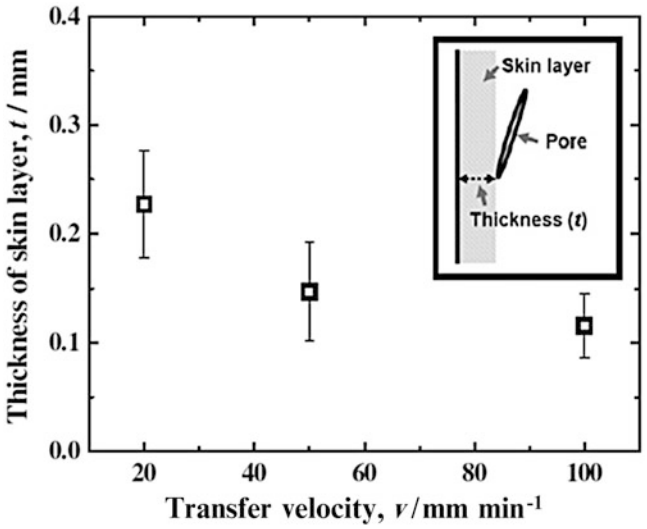

Fig. 3.21 Thickness of the skin layer plotted against the transfer velocity of lotus copper fabricated under a hydrogen gas pressure of 1.0 MPa (Reprinted with permission from [24]. © 2007 Acta Materialia Inc.)

In order to discuss the pore diameter and the pore length, the pore nucleation mechanism must be taken into consideration. Pore nucleation in the liquid has been investigated by many researchers [25, 26], and it has been reported that inhomogeneous pore nucleation occurs because the surface Gibbs free energy is lowered by the existence of impurities and inclusions. Fisher [26] suggested the following relationship between the pore nucleation rate I and the critical Gibbs free energy $(\Delta G^*_{\text{hetero}})$ for heterogeneous pore nucleation:

$$I = \frac{NkT}{h} \exp\left(-\frac{\Delta G_{\text{a}} + \Delta G^*_{\text{hetero}}}{kT}\right), \tag{3.1}$$

where N is the number of atoms in the liquid, k is Boltzmann's constant, T is the temperature, h is Planck's constant, and ΔG_{a} is the activation energy for motion of an individual atom. Here, ΔG_{a} is negligible compared to $\Delta G^*_{\text{hetero}}$, and one can obtain the expression

$$I = \frac{NkT}{h} \exp\left(-\frac{1}{kT}\frac{16\pi}{3}\frac{\gamma^3}{\Delta P^2} f(\theta_{\text{c}})\right), \tag{3.2}$$

where γ is the surface energy of the pore, ΔP is the difference between the ambient and the internal pressure of the pore, and $f(\theta_{\text{c}})$ a function of the surface energy that depends on the contact angle θ_{c} between the solid and the pore. The pore nucleation rate is closely related to ΔP, and ΔP is proportional to the undercooling ΔT through the Clausius–Clapeyron equation [27]:

$$\Delta P \propto \Delta T. \tag{3.3}$$

In addition, it is generally reported that the solidification velocity v affects the undercooling ΔT during the solidification process as follows:

$$v \propto \Delta T^n \quad (1 \leq n \leq 2), \tag{3.4}$$

where n is an empirical constant. Thus, the following expression can be finally obtained from Eqs. (3.3) and (3.4):

$$v \propto \Delta P^n. \tag{3.5}$$

Thus, the pore nucleation rate in Eq. (3.2) increases with increasing transfer velocity because of the relationship between v and ΔP in Eq. (3.5); the solidification velocity v is assumed to be equal to the transfer velocity.

On the other hand, since the hydrogen content in the melts is almost constant at the melting point under a constant hydrogen gas pressure, the hydrogen content

diffused in each pore during the solidification decreases with an increase in the pore nucleation rate. Thus, it is considered that the pore diameter decreases with a decrease in each pore volume. This is in good agreement with the results of pore length and pore aspect ratio; the changing in the pore length with the transfer velocity is similar to the change in the pore diameter, and therefore, the pore aspect ratio is not changed very much. This indicates that the pore dimensions such as diameter and length are determined by the relationship between the pore nucleation rate I and hydrogen solubility in the melt.

The pore grows in the direction perpendicular to the solid–liquid interface. Thus, the pore growth direction depends on the shape of the interface during solidification. The shape is determined by the flow of the heat emitted from the liquid during solidification. Assuming that the heat flow rate is constant in a unit area and the amount of extracted heat during solidification increases with increasing transfer velocity during unit time, it is considered that the heat extracted from the liquid at lower velocities is sufficient even at a flat interface. However, if the amount of the heat increases by an increase in transfer velocity, then a large interface area may be required at higher velocities in order to emit the additional heat. Therefore, it is thought that the interface shape changes from flat at lower velocities to concave at higher velocities. Because the depth at the center in the concave shape is proportional to the transfer velocity, the depth increases with increasing velocity. Thus, the pore growth angle shows a change such as that displayed in Fig. 3.19.

It is considered that the thickness of the skin layer is related not only to the pore growth angle but also to the distance between the pore and the surface of the slab; the thickness of the skin layer changes with a relationship of sine function between the angle and the distance as shown Fig. 3.20. The distance decreases with increasing transfer velocity as shown in Figs. 3.20 and 3.22. Assuming that the hydrogen rejected from the solid was only transported away by diffusion when solidification began, it is considered that the concentration profile of the hydrogen just before the pore formation can be expressed as shown in Fig. 3.23. There will be a buildup of the hydrogen ahead of the solid, which is accelerated by increasing solidification velocity since it is more difficult to diffuse the hydrogen from the solid to the liquid by increasing solidification velocity. If a critical hydrogen concentration $C_{\mathrm{H}}^{\mathrm{pore}*}$ for the pore formation exists, then the pore forms and grows when the hydrogen concentration ahead of the solid reaches $C_{\mathrm{H}}^{\mathrm{pore}*}$ by hydrogen buildup. When the pore is formed, the solidified distance x_c is expressed as follows [28, 29]:

$$x_c = \frac{D}{k_0 v}, \tag{3.6}$$

where D is the hydrogen diffusivity in the liquid copper at the melting point and k_0 is the equilibrium distribution coefficient; k_0 is 0.31, which is evaluated as the proportion of the hydrogen solubility in the solid and liquid copper at 1,357 K under $P_{\mathrm{H_2}} = 0.1$ MPa by using an equation suggested by Fromm and Gebhardt [30]. Assuming that the solidification velocity is equal to the transfer velocity, the

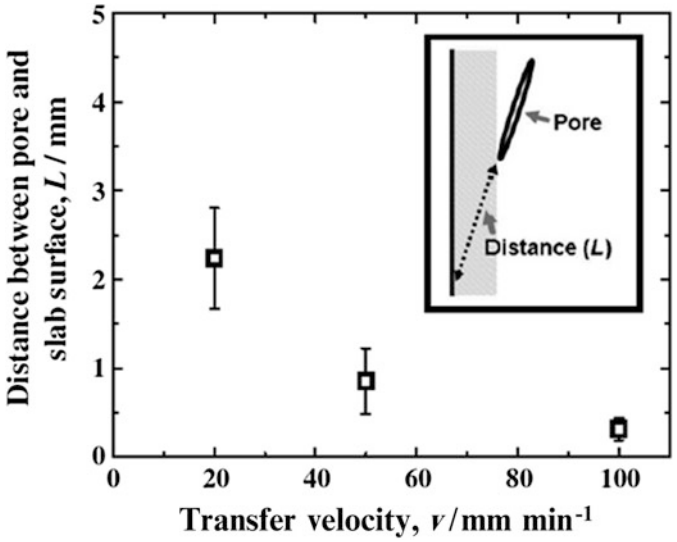

Fig. 3.22 Distance between the pore and the surface plotted against the transfer velocity of lotus copper fabricated under a hydrogen pressure of 1.0 MPa (Reprinted with permission from [24]. © 2007 Acta Materialia Inc.)

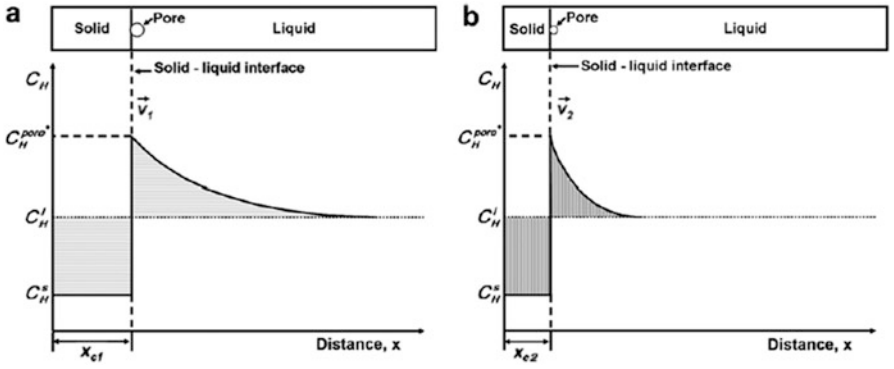

Fig. 3.23 Schematic of the hydrogen concentration profile from the beginning of solidification to pore formation in (**a**) lower solidification velocity v_1 and (**b**) higher solidification velocity v_2 (x: solidified distance, C_H^l: hydrogen concentration in liquid, C_H^s: hydrogen concentration in solid, C_H^{pore*}: critical hydrogen concentration for pore nucleation, and x_c: the solidified distance until the pore is formed) (Reprinted with permission from [24]. © 2007 Acta Materialia Inc.)

distance described in Fig. 3.22 can be plotted as a function of v^{-1}, as shown in Fig. 3.24, where the distance is in inverse proportion to the transfer velocity as shown in Eq. (3.6). The D value calculated from the slope of the dashed line is 2.28×10^{-7} m^2 s^{-1}, which is close to the value of 0.99×10^{-7} m^2 s^{-1} at 1,374 K reported by Wright and Hocking [31].

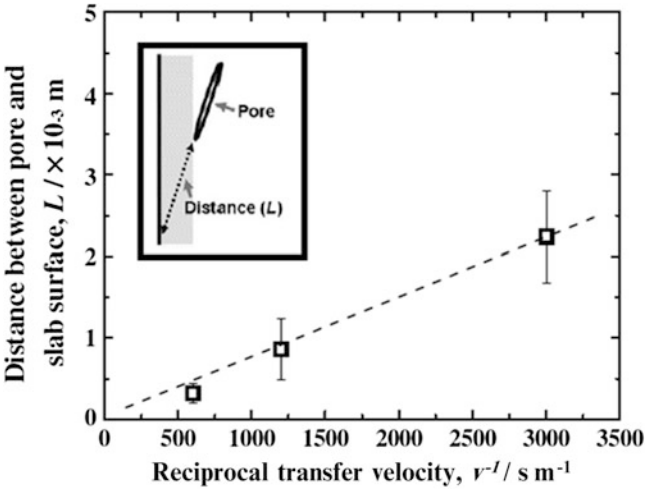

Fig. 3.24 Distance from the surface to the pore plotted as a function of reciprocal transfer velocity v^{-1} in lotus copper fabricated under a hydrogen gas pressure of 1.0 MPa (*Error bars* are the standard deviation, and the *dotted line* is the fitted line.) (Reprinted with permission from [24]. © 2007 Acta Materialia Inc.)

Consequently, the thickness of the skin layer decreases with increasing transfer velocity, which is affected by a change not only in the pore growth but also in the distance between the pore and the surface of the slab.

3.3 Thermal Decomposition Method (TDM)

As already mentioned above, the high-pressure gas method is a convenient method to supply the gas source in the molten metals for evolving gas pores in the solidified metals. However, the PGM possesses two disadvantages: (1) necessity of strongly built high-pressure chamber and application of high-pressure regulation and (2) necessity of safety procedure to protect against hydrogen as an inflammable and explosive gas. Mass production and commercialization in industries are hesitated from such disadvantages. Therefore, a technique that does not require high-pressure hydrogen to fabricate lotus metals is highly desirable. In order to overcome these difficulties, Nakajima group [32] proposed an alternative, but simple, method to fabricate such lotus metals by using a thermal decomposition method (TDM) of compounds containing gas elements in a non-hydrogen atmosphere under nearly atmospheric pressure.

The compounds suitable for TDM can be listed up to the following [33]:

TiH_2, MgH_2, ZrH_2, Fe_4N, TiN, Mn_4N, CrN, Mo_2N, $Ca(OH)_2$, Cu_2O, B_2O_3, $CaCO_3$, $SrCO_3$, $MgCO_3$, $BaCO_3$, and $NaHCO_3$.

The compounds should be decomposed into gas element and another type of metallic compound at the temperature (dissolving temperature) just below the melting point of the solvent metal to be solidified. If the dissolving temperature of the compounds is higher than the melting point of the metal, sufficient dissolution of the gas element into the melt cannot be ensured. The principle of TDM and the first versatile method to control the pore morphology, including pore size and porosity of lotus metals are described.

3.3.1 Mold Casting Technique through TDM

3.3.1.1 Fabrication of Lotus Copper through TDM

Copper (99.99 % pure) was melted by radio-frequency induction heating in a graphite crucible under an argon atmosphere from 0.1 to 0.5 MPa. The melt was poured into the mold, which had a copper bottom plate cooled by water and lateral side walls made of 0.1-mm-thick cylindrical stainless steel. A few pellets of titanium hydride, which ranged between 0.075 and 0.25 g in mass for melting copper of 200 g, were set on the bottom plate of the mold. Unidirectional solidification occurred in the mold so that a lotus copper ingot was obtained, as illustrated in Fig. 3.25a. The ingot size was 28 mm in diameter and had a height of maximum 90 mm. The ingot was cut by a spark-erosion wire-cutting machine parallel and perpendicular to the solidification direction.

Another method was also used to supply the hydrogen source in the melt. As shown in Fig. 3.25b, a few pellets of titanium hydride were set in the crucible along with copper. During the copper melt, hydrogen, which decomposed from titanium hydride, was dissolved into the melt. The molten copper was poured from the crucible into the mold without pellets of titanium hydride for unidirectional solidification. The ingots were investigated using the same method described previously.

Figure 3.26 shows the optical micrographs of the cross-sectional views of lotus copper parallel and perpendicular to the solidification direction [32]. The pore growth direction is coincident to the direction of the unidirectional solidification, which is in agreement with that of the conventional high-pressure gas method (PGM). Therefore, the principal mechanism of this pore evolution is suggested to be similar to that of PGM; when the molten metal dissolving a gas is solidified, insoluble gas precipitates and evolves the gas pores in the solid metals.

Figure 3.27 shows dependence of the porosity and the average pore diameter on the mass of titanium hydride for the lotus copper fabricated by TDM in a 0.1 MPa argon atmosphere. The porosity abruptly increases by the addition of 0.10 g of titanium hydride and becomes constant to be about 55 % in the porosity on further addition. When 0.10 g of titanium hydride was added to 200 g of molten copper, the concentration of hydrogen in the melt was evaluated as 0.128 at. pct. Directly comparing the hydrogen concentration from the titanium hydride to the available data on the solubility in molten copper just above the melting temperature (T_m),

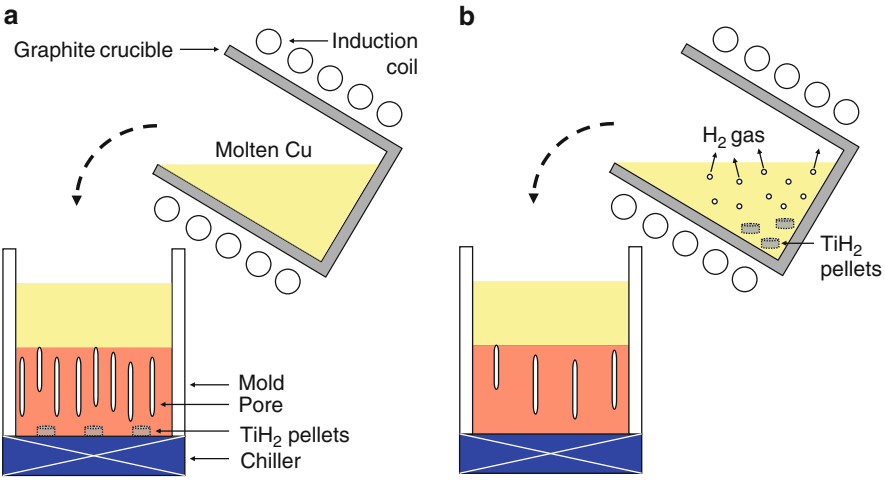

Fig. 3.25 Schematic drawings of the principle to fabricate lotus metals by a mold casting technique: (**a**) pellets of titanium hydride are set in the mold and (**b**) pellets of titanium hydride are set in the crucible (Reprinted with permission from [32]. © 2008 The Minerals, Metals & Materials Society and ASM International)

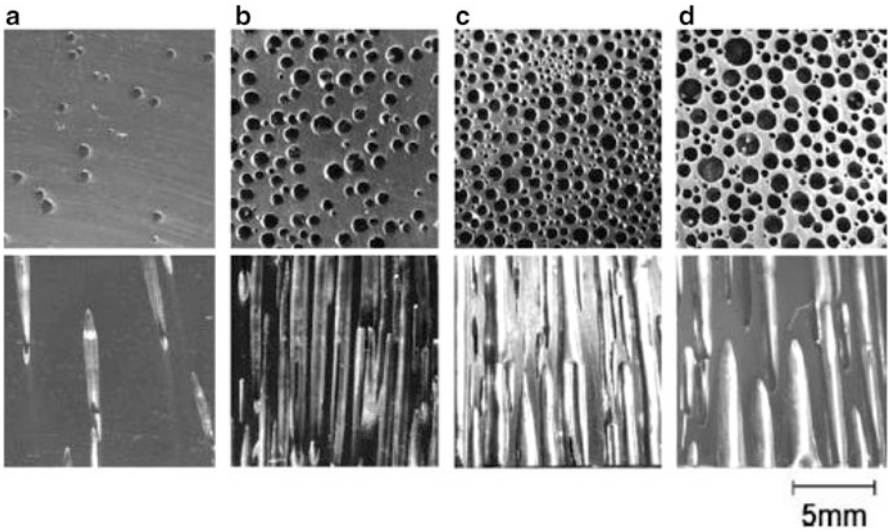

Fig. 3.26 Optical micrographs of cross-sectional views of lotus copper (*upper views*) perpendicular and (*lower views*) parallel to the solidification direction. Mass of titanium hydride added to the mold is (**a**) 0.075 g, (**b**) 0.10 g, (**c**) 0.125 g, and (**d**) 0.25 g. Melting and subsequent solidification were carried out in 0.1 MPa argon atmosphere (Reprinted with permission from [32]. © 2008 The Minerals, Metals & Materials Society and ASM International)

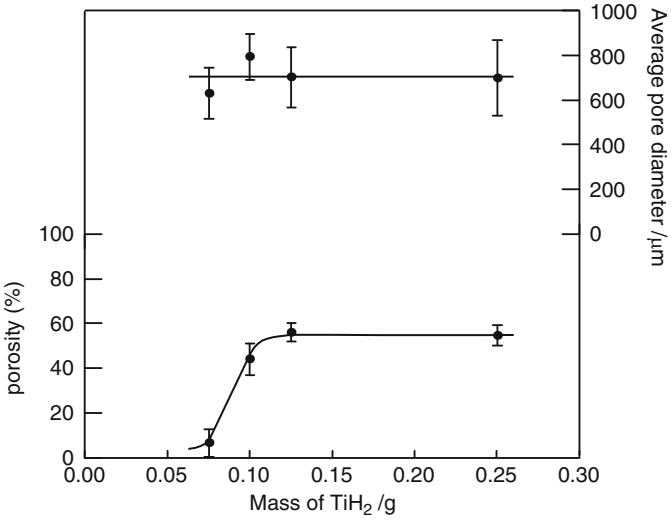

Fig. 3.27 Dependence of the porosity and the average pore diameter on the mass of titanium hydride. Melting and subsequent solidification were carried out in 0.1 MPa argon atmosphere (Reprinted with permission from [32]. © 2008 The Minerals, Metals & Materials Society and ASM International)

1,083 K, is impossible, because the atmospheric hydrogen pressure of the TDM process differs from that of the solubility measurement (0.1 MPa). However, the concentration of dissolving hydrogen in the TDM process is comparable to the solubility of hydrogen in the liquid phase of copper near T_m [30]. If more than 0.1 g of titanium hydride is added to the melt, the supersaturated hydrogen may generate gas bubbles, which are then liberated from the melt to the atmosphere. The hydrogen dissolved in the melt evolves pores at the solid–liquid interface during solidification. If less than 0.1 g of titanium hydride is added, then all hydrogen can dissolve in the melt without bubbling so that some of the hydride forms pores in the solid–liquid interface, but the porosity may be smaller than that when more than 0.1 g of the hydride is added. Such redistribution of hydrogen in the liquid phase to the solid phase and the atmosphere is exhibited in Fig. 3.28a, b, depending on the mass of titanium hydride. For comparison, Fig. 3.28c shows the PGM case. The TDM process is based on a nonequilibrium state, while the PGM process is based on an equilibrium state in the chamber where a constant high-pressure gas is maintained. On the other hand as shown in Fig. 3.27, the average pore diameter is constant and nearly independent of the mass of titanium hydride. It has been previously confirmed that the pore size is affected by the supercooling rate from the liquid to the solid, which can be controlled by the solidification velocity in the PGM [19, 23, 24]. The same reasoning can be used to interpret the present data.

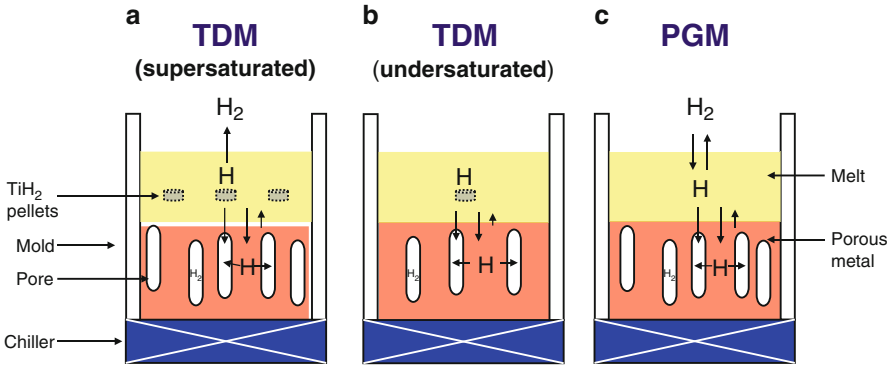

Fig. 3.28 Schematic drawings of the redistribution of hydrogen dissolved in the melt to the solid phase and atmosphere. (**a**) Thermal decomposition method: the melt contains supersaturated hydrogen. (**b**) Thermal decomposition method: the melt contains undersaturated hydrogen. (**c**) High-pressure gas method. In all cases, hydrogen dissolved in the melt near the solid–liquid interface moves directly into the pores, but some of the hydrogen moves in the solidified metal, while insoluble hydrogen diffuses into the pores via the solid or diffuses back to the melt (Reprinted with permission from [32]. © 2008 The Minerals, Metals & Materials Society and ASM International)

Next, the atmospheric pressure effect was investigated. For this study, the mass of titanium hydride was constant at 0.25 g, and argon was selected as the atmospheric gas, which served as the external pressure. The argon pressure was varied from 0.1 to 0.5 MPa. Figure 3.29 shows sectional views of lotus copper parallel and perpendicular to the solidification direction as a function of argon pressure. The effect of external pressure is obvious, and the pore growth is suppressed at higher pressure. Figure 3.30 shows the dependence of the porosity and the average pore diameter as a function of argon pressure. Both the porosity and the average pore diameter decrease with increasing argon pressure. The pore volume v, which is equal to the porosity, is inversely proportional to the external argon pressure P, which can be described by the Boyle–Charles law, $v = nRT/P$, where n, R, and T are the hydrogen molar number, the gas constant, and the temperature, respectively. Therefore, the pore diameter can be written as $d \propto P^{-1/3}$. The tendency of the pressure dependence of the porosity and the pore diameter are explained by the law. However, it seems that such a pressure effect may be more significant than that predicted by the Boyle–Charles law. This difference may be attributed to the possibility that the molar number of hydrogen is not constant under changing pressure. The decomposition rate of titanium hydride should be retarded as the external pressure of argon increases. Thus, the porosity and the pore diameter may decrease remarkably.

Finally, we examined the role of the other metallic element, Ti, through the thermal decomposition of titanium hydride. Titanium hydride is decomposed into hydrogen and titanium. The latter is a very reactive element, which easily reacts with residual oxygen in the molten copper. Consequently, titanium oxide particles are formed and dispersed, which may serve as the nucleation sites for the hydrogen

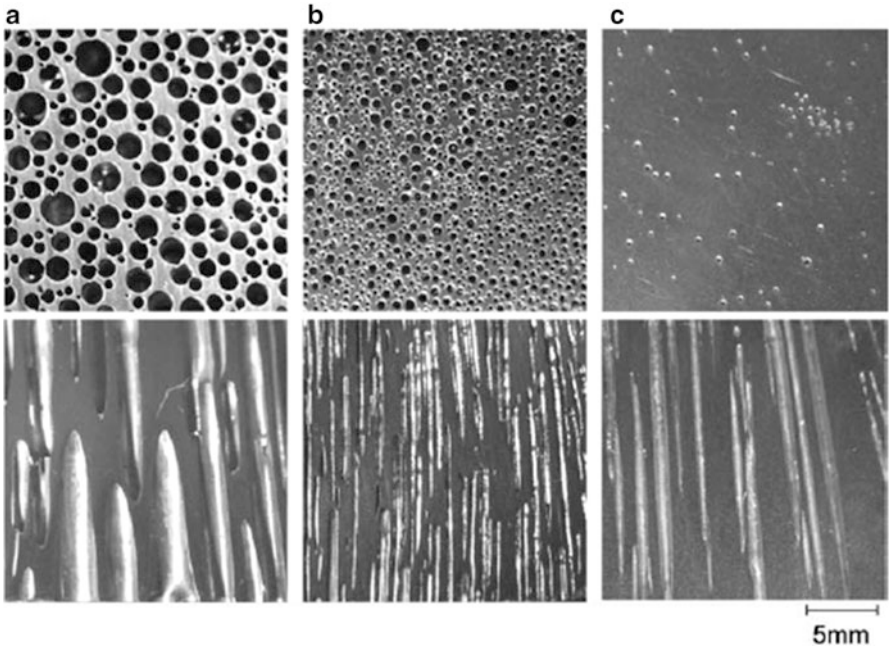

Fig. 3.29 Cross-sectional views of lotus copper fabricated under different argon pressure. (**a**) 0.1 MPa, (**b**) 0.25 MPa, and (**c**) 0.5 MPa. *Upper* and *lower views* are the cross section perpendicular and parallel to the solidification direction, respectively. Titanium hydride (0.25 g) was added to the mold during solidification (Reprinted with permission from [32]. © 2008 The Minerals, Metals & Materials Society and ASM International)

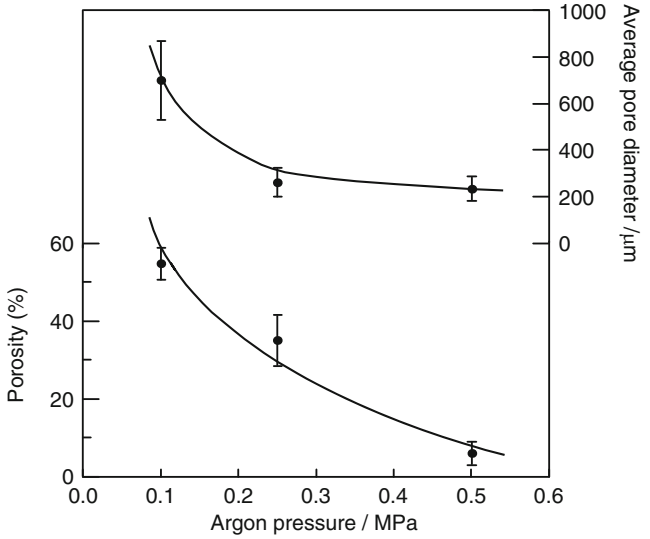

Fig. 3.30 Dependence of the porosity and the average pore diameter on argon pressure. Titanium hydride (0.25 g) was added to the mold during solidification (Reprinted with permission from [32]. © 2008 The Minerals, Metals & Materials Society and ASM International)

pores in the solid–liquid interface during unidirectional solidification. It is well known that the pores evolve by heterogeneous nucleation in metal melts in the presence of small amounts of foreign particles [34]. Therefore, the same reasoning can be applied to the present case, and it is surmised that the pore size and porosity become homogeneous by uniformly distributed nucleation sites. Thus, TDM exhibits another advantage to produce lotus metals with more homogeneous pore size and porosity than those by PGM, which does not provide intentional nucleation sites.

3.3.1.2 Fabrication of Lotus Aluminum through TDM

The investigation was undertaken to fabricate lotus aluminum with the porosity more than 10 % through TDM [35]. For this purpose, three types of the compounds containing hydrogen were used: calcium hydroxide, sodium bicarbonate, and titanium hydride. The pore morphology is usually characterized with the pore size and porosity, which were controlled by the temperature of melt, amount of compounds, and external argon pressure in this work.

Pure aluminum (99.99 % pure) of about 100 g was melted in a graphite crucible by an induction heating coil in vacuum. The bottom of the mold was copper plate cooled by a circulated water chiller, while the side was made of stainless steel. 0.2 g of the compounds such as calcium hydroxide, sodium bicarbonate, or titanium hydride was usually wrapped with aluminum foil and was set on the bottom plate of the mold. The temperature of the liquid in the graphite crucible was monitored by an infrared pyrometer. After pouring the molten aluminum at 1,023 K in the crucible into the mold, hydrogen decomposed from the compounds dissolves in the melt, which is then solidified so that insoluble hydrogen precipitates to evolve the hydrogen pores. In order to investigate the dependence of the pore size and porosity on the mass of calcium hydroxide, the amount of compounds was changed from 0.1 to 1.0 g. In order to investigate the external pressure dependence of the pore size and porosity, the argon pressure was changed from vacuum to 0.04 MPa.

When the solidification took place unidirectionally, lotus aluminum with directional cylindrical pores was fabricated. The size of the obtained ingot was about 25 mm in diameter and about 60 mm in height. The specimens were cut using a spark-erosion wire-cutting machine in both directions parallel and perpendicular to the solidification direction. Each cross section was polished with a series of emery papers and was observed using an optical microscope.

The constituent elements of pores were investigated using gas analyzers. After the specimen kept into salt-saturated distilled water was cut, the gas bubbles were collected into a vial in the distilled water. The collected gas was analyzed by a gas chromatograph (GC-14A, Shimadzu Co., Kyoto, Japan) in order to identify hydrogen, carbon monoxide, and carbon dioxide. Oxygen was analyzed by a gas analyzer (TC-300, LECO Co., St. Joseph, MI).

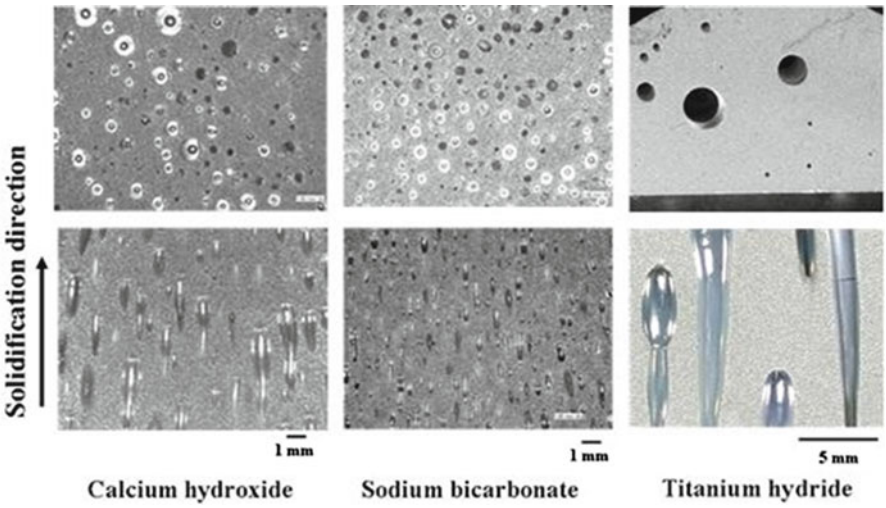

Fig. 3.31 Optical micrographs of lotus aluminum fabricated by mold casting technique with different compounds in vacuum at 1,023 K. The *upper* and *lower* micrographs are the cross sections perpendicular and parallel to the solidification direction, respectively (Reprinted with permission from [35]. © 2009 The Minerals, Metals & Materials Society and ASM International)

Figure 3.31 shows the microstructure of lotus aluminum on cross sections parallel and perpendicular to the solidification direction. The pore morphologies perpendicular to the solidification direction are shown on the upper photos, while those parallel to the solidification direction are shown in the lower photos. In all specimens, the aligned pores parallel to the solidification direction were observed. It is considered that the cylindrical gas pores are evolved by TDM from the compounds during solidification of aluminum containing hydrogen gas.

Table 3.2 compiled the decomposition reactions of three compounds in the aluminum melt. Calcium hydroxide and sodium bicarbonate decompose into vapor and compounds and then, the vapor decomposes to hydrogen and metallic oxide. On the other hand, titanium hydride decomposes into hydrogen and titanium. These decomposed gas elements can dissolve in aluminum melt. When the melt is solidified, lotus aluminum can be produced.

Figure 3.32 shows the pore size and porosity of lotus aluminum with different compounds using the mold casting technique in vacuum. It is seen that the pores with average size 400, 268, and 1,086 μm are evolved by using calcium hydroxide, sodium bicarbonate, and titanium hydride, respectively. The porosity of lotus aluminum was similar, being as much as 20 % regardless of the kinds of the compounds. The pore size was small, as much as 400 μm, and its distribution was homogeneous in porous aluminum through TDM of calcium hydroxide and sodium bicarbonate, while the pore size was large as much as 1,000 μm and its distribution is not uniform through the TDM of titanium hydride.

Table 3.2 Decomposition reaction and temperature of gas-forming compounds

Reactions	Decomposition temperature (K)	Gas atoms or molecules to be dissolved
$Ca(OH)_2 \rightarrow CaO + H_2O$ $H_2O \rightarrow$ metallic oxide + 2H	853	H
$2NaHCO_3 \rightarrow Na_2CO_3 + H_2O + CO_2$ $H_2O \rightarrow$ metallic oxide + 2H	473	H, CO, CO_2, O
$TiH_2 \rightarrow Ti + 2H$ $Ti \rightarrow$ dissolved in liquid	723	H

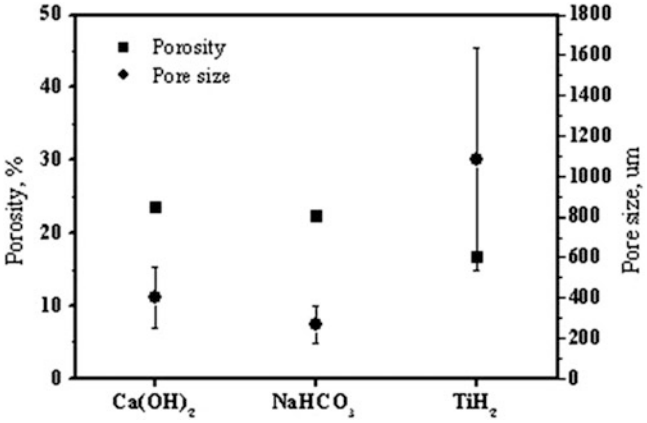

Fig. 3.32 Pore size and porosity of lotus aluminum fabricated by mold casting technique using compounds in vacuum (Reprinted with permission from [35]. © 2009 The Minerals, Metals & Materials Society and ASM International)

Calcium hydroxide or sodium bicarbonate decomposes into compounds (CaO, Na_2CO_3), carbon dioxide, and vapor, the latter of which furthermore decomposes into metallic oxide and hydrogen. Small pore size with homogeneous distribution was observed through these reactions. On the other hand, titanium hydride decomposes directly into titanium and hydrogen. Large pores with inhomogeneous distribution were observed. It is not clear at present, but evolution of small pores with homogeneous distribution may be attributed to the existence of the oxide particles, which may serve as the nucleation sites of the pores. In order to investigate the content of pore gas, the gas analysis was carried out. Figure 3.33 shows the results of gas analysis of lotus aluminum using different compounds. It can be seen that hydrogen was the pore-formation source in the case of titanium hydride, calcium hydroxide, and sodium bicarbonate. Although the absolute values of concentration of each gas element cannot be compared in the analysis, it is apparent that the major gas is hydrogen in three kinds of the specimens. The contents of

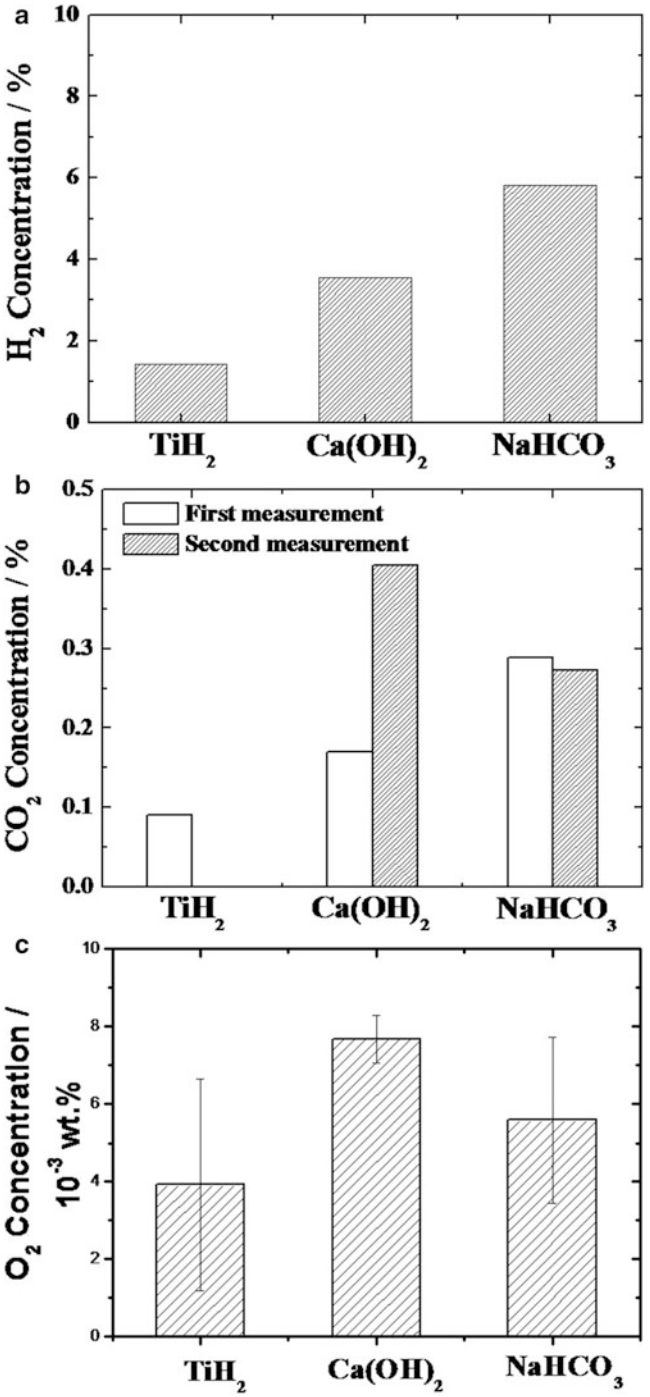

Fig. 3.33 Results of gas analysis in the pore in lotus aluminum. (**a**) Hydrogen, (**b**) carbon dioxide, and (**c**) oxygen (Reprinted with permission from [35]. © 2009 The Minerals, Metals & Materials Society and ASM International)

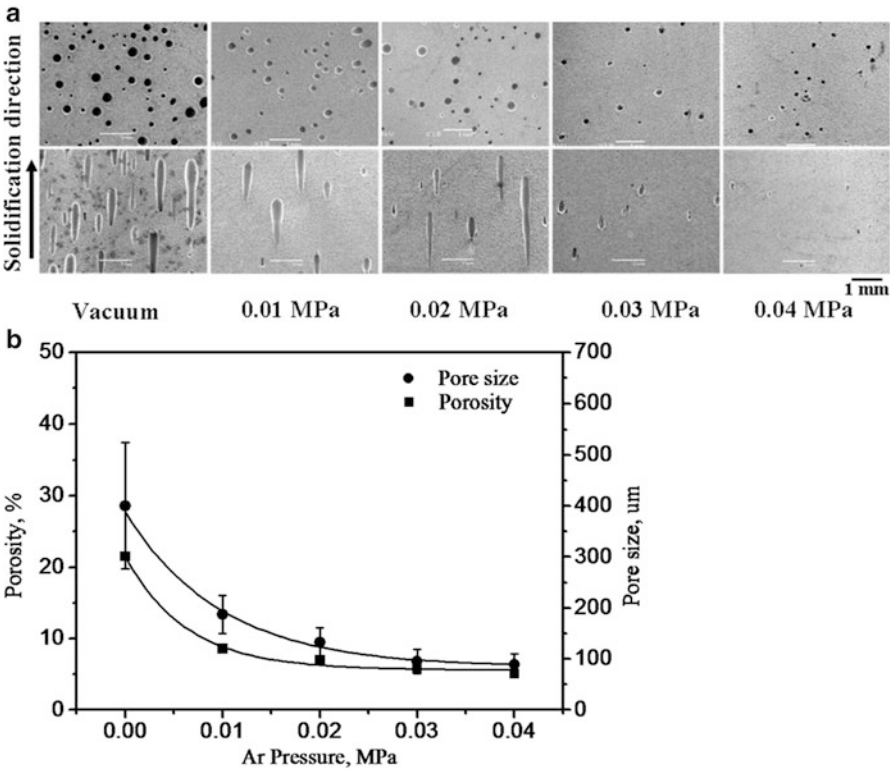

Fig. 3.34 Lotus aluminum fabricated using calcium hydroxide in vacuum or under argon pressure (0.01–0.04 MPa). The amount of calcium hydroxide was kept to be 0.2 g. (**a**) Pore morphology. The *upper* and *lower* micrographs are the cross sections perpendicular and parallel to the solidification direction, respectively. (**b**) Variation of the porosity and pore size as a function of argon pressure (Reprinted with permission from [35]. © 2009 The Minerals, Metals & Materials Society and ASM International)

oxygen and carbon dioxide are very small; some amount of them may be contained in the collection handling procedure of the pores.

Figure 3.34a shows the pore structures on cross sections of lotus aluminum perpendicular (upper) and parallel (lower) to the solidification direction. The lotus aluminum was fabricated using calcium hydroxide in vacuum and under argon atmosphere. The aligned pores formed under the pressure less than 0.03 MPa Ar; however, spherical pores formed over 0.04 MPa argon. This may indicate that the applied pressure in the chamber reduces the driving force for pore nucleation and growth. Figure 3.34b shows the dependence of the porosity and the average pore size as a function of argon pressure. The effect of external pressure is obvious, and the pore growth is suppressed under higher pressure. Both the porosity and the average pore size decrease with increasing argon pressure. The pore volume v,

which is equal to the porosity, is inversely proportional to the external argon pressure P, which can be described by the Boyle law, $v = nRT/P$, where n, R, and T are the hydrogen molar number, the gas constant, and the temperature, respectively. Therefore, the pore diameter can be written as $d \propto P^{-1/3}$. The tendency of the pressure dependence of the porosity and pore size are explained by the law.

3.3.2 Continuous Zone Melting Technique through TDM

Recently, Makaya and Fredriksson produced porous Fe-based materials by dissolving CrN compound into a metallic melt of Fe-based alloy in an argon atmosphere [36]. The decomposition of the compound leads to dissolution of a gas into the melt. They solidified the melt in the crucible to produce porous metals with an isotropic pore structure. However, no investigations were carried out to produce porous metals with an anisotropic cylindrical pore structure until Nakajima and Ide performed theirs. Nakajima and Ide studied fabrication of lotus copper using titanium hydride in an argon atmosphere instead of a pressurized hydrogen atmosphere, which is called as TDM [32]. In order to fabricate the lotus metals, unidirectional solidification was usually carried out using the mold casting technique, as mentioned already. However, this technique cannot be applied to the metals and alloys with low- thermal conductivity. The solidification rate changes from the bottom to the top: the cooling speed near the bottom is faster, while it becomes slower near the top where the pore is coarsened because the heat cannot be dissipated. Thus, the pore size significantly changes with the height; the pore size increases with increasing height of the mold. In order to solve this problem, Ikeda et al. developed a continuous zone melting technique [23]. The partial melting zone is moved to retain the constant solidification velocity so that uniform distribution of porosity and pore size are obtained. This technique was adopted to fabricate lotus iron by Wada et al. [37].

Iron rods of 10.0 mm in diameter and 80 mm in length were used as specimens. In order to supply a constant source of chromium nitride, a hole of 2.0 mm in diameter in a central part of the cross section was made by an electric drill as shown in Fig. 3.35. The compound was filled into the hole. The chromium nitride was selected as a gas dissolving compound, since the temperature of gas releasing chromium nitride is the closest to the melting temperature of iron. The $Cr_{1.18}N$ and Cr_2N powders were used. The former was a mixture of 81.4 mass pct CrN and 18.6 mass pct Cr_2N. 1.0 mass pct of $Cr_{1.18}N$ powders was filled into the permeable straight hole of the iron rods. The continuous zone melting was carried out by controlling the transfer velocity from 80 to 580 μm s^{-1}.

Figure 3.36 shows the cross-sectional views of lotus iron perpendicular and parallel to the solidification direction as a function of the transfer velocity. No pores were observed in the ingot fabricated with the velocity of 80 μm s^{-1}. Figure 3.37 exhibits the transfer velocity dependence of the porosity and average pore diameter. The porosity increases with increasing transfer velocity, while the variation of the

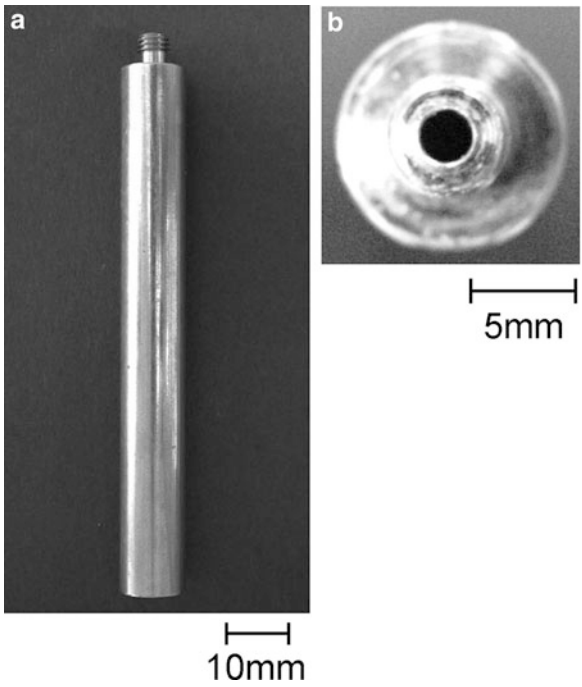

Fig. 3.35 Outer view of iron rod: (**a**) longitudinal direction and (**b**) cross section perpendicular to the longitudinal direction (Reprinted with permission from [37]. © 2009 The Minerals, Metals & Materials Society and ASM International)

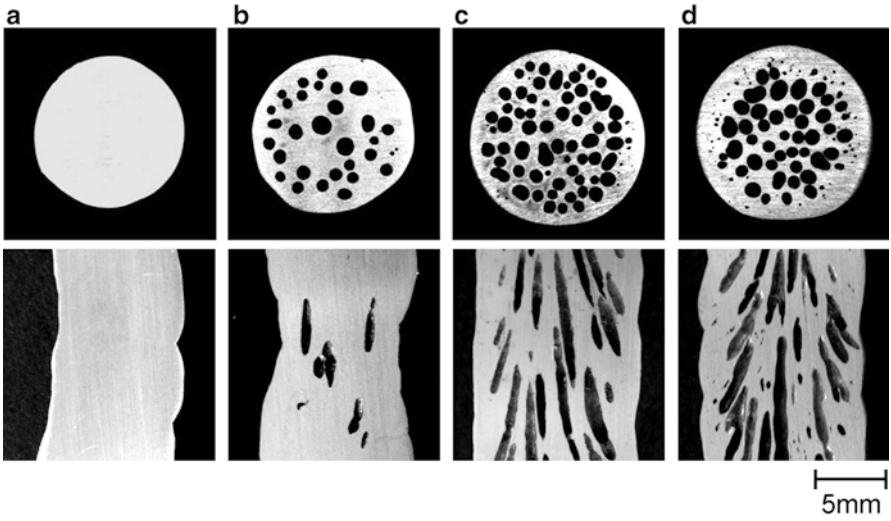

Fig. 3.36 Cross-sectional views of lotus iron perpendicular (*upper*) and parallel (*lower*) to the solidification direction. Transfer velocity: (**a**) 80 μm s^{-1}, (**b**) 250 μm s^{-1}, (**c**) 410 μm s^{-1}, and (**d**) 580 μm s^{-1}. Atmosphere is 0.5 MPa helium (Reprinted with permission from [37]. © 2009 The Minerals, Metals & Materials Society and ASM International)

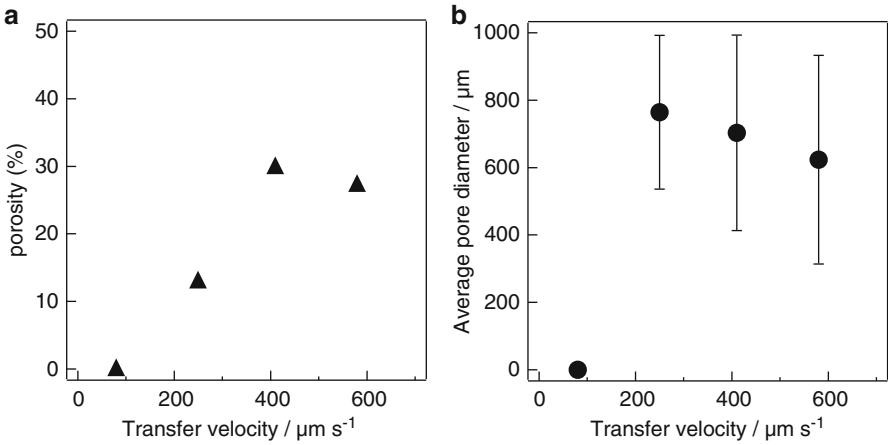

Fig. 3.37 Transfer velocity dependence of (**a**) the porosity and (**b**) average pore diameter of lotus iron. Atmosphere is 0.5 MPa helium (Reprinted with permission from [37]. © 2009 The Minerals, Metals & Materials Society and ASM International)

pore diameter with the velocity is relatively limited compared with previous results [23, 24]. This suggests that the mechanism of pore formation obtained by this study by TDM is different from that obtained by PGM.

In the mold casting, the gas compound reacts and simultaneously dissolves a gas into the melt during the casting without preheating of the gas compound. However, in the continuous zone melting, when the rod is solidified unidirectionally, it is preheated by heat conduction before melting so that it has a temperature distribution. In general, the behavior of thermal decomposition of compounds is strongly affected by the heating rate [38]. The possibility of forming pores by continuous zone melting will be discussed, taking into consideration the transfer velocity dependence of the temperature distribution in the iron rod and the thermal decomposition of nitride. The relation between the temperature T of preheated rod and the distance x from the solid–liquid interface under the transfer velocity v can be expressed by applying an equation of redistribution of solute in material solidified in the zone melting at constant velocity to a heat conduction [39].

$$\frac{d}{dx}\left(\lambda\frac{dT}{dx}\right)+\rho cv\frac{dT}{dx}=0, \tag{3.7}$$

where ρ, c, and λ are the density of iron, the specific heat of iron, and the thermal conductivity of iron, respectively. Figure 3.38 shows the temperature and the heating rate as a function of the distance from the interface between liquid and solid at different transfer velocities. Both the temperature gradient and heating rate increase with increasing transfer velocity. Therefore, it is considered that the position in the rod where the gas is released from chromium nitride varies with the transfer velocity.

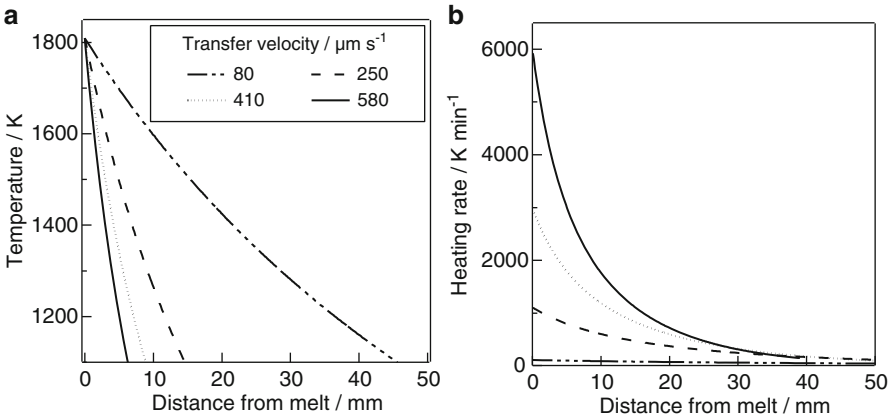

Fig. 3.38 Changes in (**a**) temperature and (**b**) heating rate as a function of the distance from the interface between liquid and solid at different transfer velocities (Reprinted with permission from [37]. © 2009 The Minerals, Metals & Materials Society and ASM International)

Derivative thermogravimetry (DTG) of chromium nitrides of $Cr_{1.18}N$ and Cr_2N powders was carried out using a thermal analyzer in an argon flow of 0.1 MPa in the temperature range from room temperature to 1,773 K. The heating rate was changed from 10, 20, 30, and 40 K min^{-1}. Figure 3.39 shows DTG curves with the heating rate of 10 K min^{-1} for $Cr_{1.18}N$ and Cr_2N powders. Two peaks for gas release from $Cr_{1.18}N$ were observed at 1,240 K(T_{p1}) and 1,570 K(T_{p2}), while one peak from Cr_2N was found at 1,680 K. Thus, the 1,570 K peak observed in higher temperature is attributed to the gas release from Cr_2N. Since $Cr_{1.18}N$ is composed of CrN and Cr_2N, the 1,240 K peak of lower temperature is due to the gas release from CrN. According to the DTG measurement of $Cr_{1.18}N$ at different heating rate, the starting temperature and peak temperature of the gas release are shifted to higher temperature with increasing heating rate.

According to Kissinger [40], the heating rate β is related to the peak temperature T_p for gas release by the following equation:

$$\frac{d\ln\left(\frac{\beta}{T_p^2}\right)}{d\left(\frac{1}{T_p}\right)} = -\frac{E_a}{R}, \tag{3.8}$$

where E_a is an activation energy of reaction and R is the gas constant. The Kissinger plots of the peak temperature were obtained from the measured DTG curves. It is predicted from the plots that the heating rates with which the peak temperature for the gas release is equal to the melting temperature (1809 K) of iron are 3.58×10^4 K min^{-1} ($H.R_1$) for CrN and 5.70×10^2 K min^{-1} ($H.R_2$) for Cr_2N. In order to have decomposition of the nitrides into the melt, the transfer velocity has to be such that the heating rate in the rod exceeds the predicted value, while there is an optimal heating rate. Figure 3.40 shows the relation between the temperature of the rod and

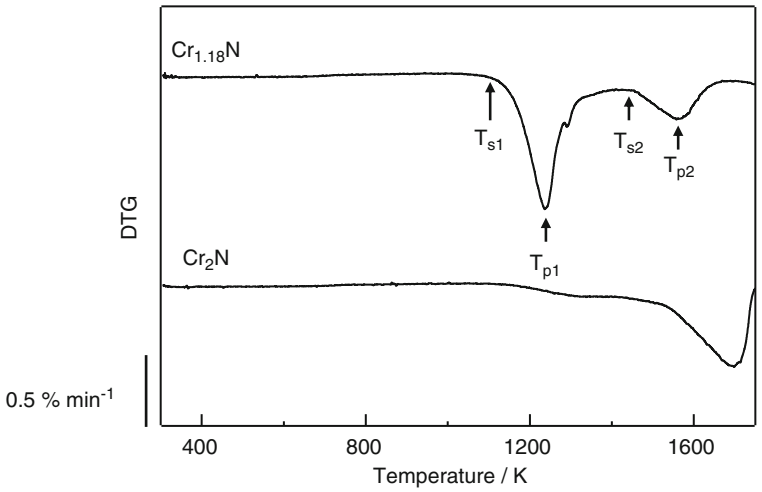

Fig. 3.39 DTG curves measured by the DTG with the heating rate of 10 K min^{-1} for $Cr_{1.18}$ N and Cr_2N powders. The T_s and T_p are the starting temperature and peak temperature of the gas release, respectively (Reprinted with permission from [37]. © 2009 The Minerals, Metals & Materials Society and ASM International)

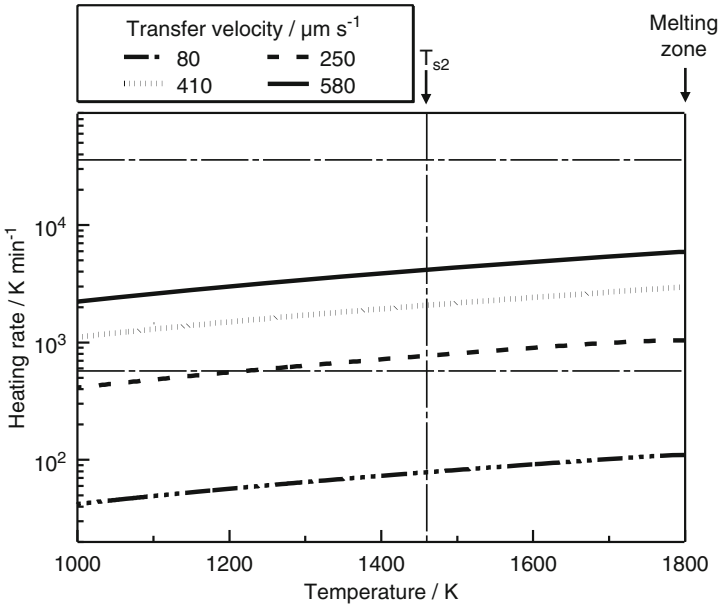

Fig. 3.40 Relation between heating rate and temperature of the rod at different transfer velocities (Reprinted with permission from [37]. © 2009 The Minerals, Metals & Materials Society and ASM International)

heating rate, which is obtained from the results of Fig. 3.38a, b. Since the predicted $H.R_1$ is higher than the heating rates at all transfer velocity, gas from CrN contained in $Cr_{1.18}N$ is released before melting and does not contribute to pore evolution. On the other hand, $H.R_2$ in higher temperature than the starting temperature (about 1,450 K slightly depending on the heating rates) for gas release is slower than the heating rates in the transfer velocity more than 250 μm s^{-1}. Therefore, it is surmised that no pore formation at lower transfer velocity of 80 μm s^{-1} is attributed to insufficient nitrogen release into the molten iron, because most of nitrogen gas released from the nitride escapes to the atmosphere; the rod is heated at high temperature by heat conduction from the melt part of a longer time. It is considered that gas from Cr_2N contained in $Cr_{1.18}N$ cannot be released until part of the rod melts and is used effectively to evolve the pores. Thus, for transfer velocity such that the decomposition peak temperature lies just above the melting point, decomposition of the nitrides in the melt is optimal.

Different from PGM, a gas equilibrium between the atmosphere (nitrogen partial pressure ~ 0) and the melt is not maintained in TDM [32]. During melting, nitrogen escapes from the melt to the atmosphere. Since the holding time of the melting condition decreases with increasing transfer velocity, the amount of escaped nitrogen may decrease; thus, the porosity increases with increasing transfer velocity, as shown in Fig. 3.37a.

3.3.3 Continuous Casting Technique through TDM

As mentioned above, TDM is desirable to avoid inherent risk of employing high-pressure hydrogen gas, and the continuous casting technique is suitable to produce large-sized lotus metal slabs with controllable pore size and porosity. Combining both techniques is the most suitable to fabricate lotus metals. Nakajima and Ide [41] fabricated long-sized lotus copper slabs through TDM by continuous casting technique. Figure 3.41a illustrates the continuous casting apparatus for TDM; for comparison, the apparatus of continuous casting technique through PGM is shown in Fig. 3.41b. The apparatus consists of three parts. (1) The first part is the melting part; the copper were melted in the graphite crucible by the induction heating. The upper cylindrical graphite bar was pushed down. (2) The overflowing copper melt dropped down into a tundish, in which pellets of titanium hydride were supplied through a nozzle at a constant time interval in order to maintain the dissolving hydrogen constant. (3) The third part is the mold cooled by water and pinch rollers which pulled the dummy bar and the solidified slab ingot horizontally. Figure 3.42 shows one example of lotus copper fabricated with addition of a pellet, 0.2 g, per minute at the melt temperature of 1,573 K in argon atmosphere of 0.1 MPa with different transfer velocity. The concentration of titanium hydride in the melt added in the tundish was evaluated as 0.001mass%. Almost uniform pore distribution in size and position was observed in the cross section parallel to the

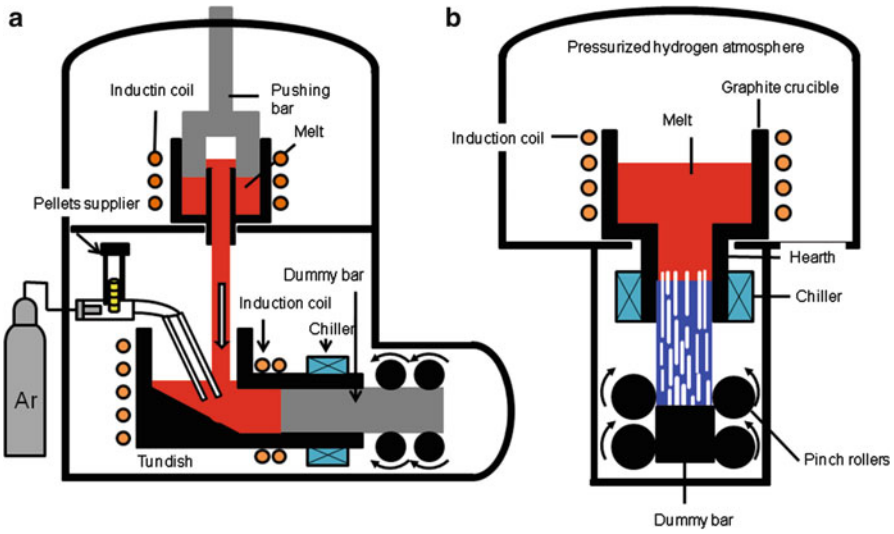

Fig. 3.41 Apparatus of continuous casting technique to fabricate lotus metals through (**a**) TDM and (**b**) PGM (Reprinted with permission from [41]. © 2012 Deutsche Gesellschaft fur Materialskunde e.V.)

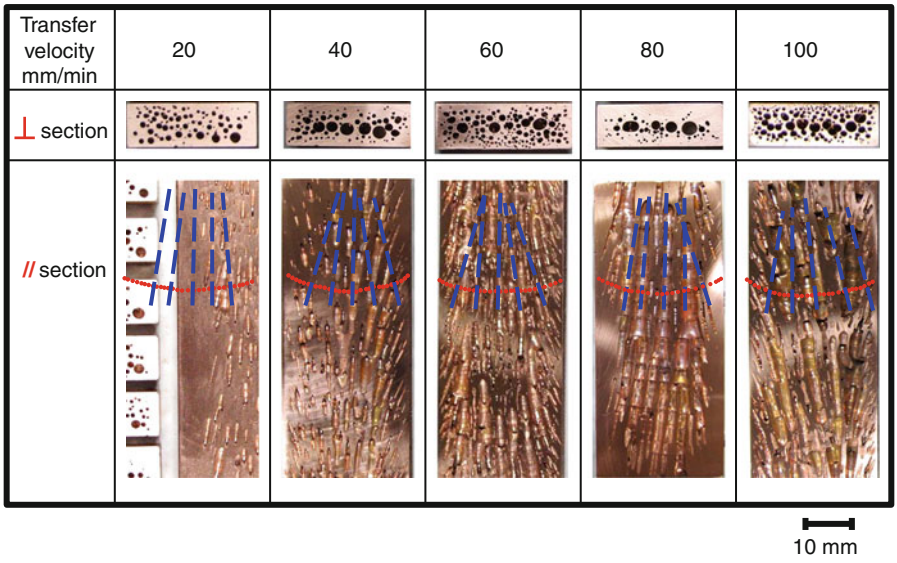

Fig. 3.42 Lotus copper fabricated by continuous casting technique through TDM. *Upper* and *lower* are the cross sections perpendicular and parallel to the solidification direction, respectively

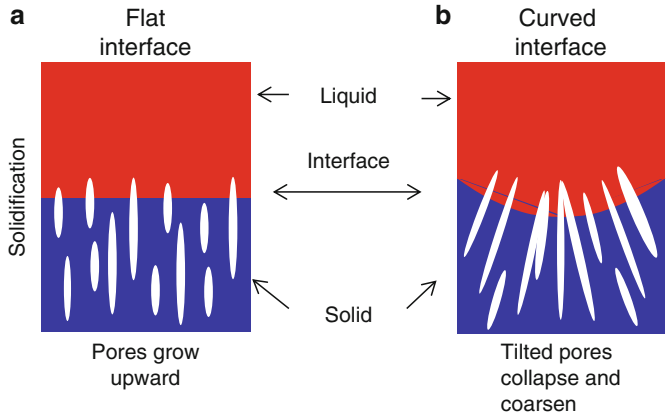

Fig. 3.43 Relation between alignment of evolving pores and the shape of liquid–solid interface. (**a**) The alignment of the evolving pores is unidirectional. (**b**) The alignment is tilted. The tilted pores collapse to coarse pores in the central part

solidification direction, but not uniform in the section perpendicular. This is because tilted pores collapsed to cause coarse pores in the central part, as shown in Fig. 3.43b. The alignment of the evolving pores should be unidirectional as shown in Fig. 3.43a. If a flat liquid–solid interface can be obtained by controlling the chiller temperature in the hearth, this problem will be solved.

3.4 Moisture Decomposition Method

3.4.1 Fabrication of Lotus Nickel by Moisture

Lotus nickel was successfully fabricated by unidirectional solidification using molybdenum-sheet mold coated by Al_2O_3–Na_2SiO_3 in an argon atmosphere. During solidification, the moisture absorbed in Al_2O_3–Na_2SiO_3 at atmospheric temperature is dissolved into the melt and then the gas pores are formed at the solid–liquid interface. Nickel in a magnesia crucible was melted by induction heating at a given pressure of argon gas in the high-pressure chamber. As shown in Fig. 3.44, the molten nickel was poured into the mold whose bottom was water-cooled by a chiller from the crucible. The mixture paste of alumina, sodium silicate, and water was coated on the inside lateral surface on the molybdenum cylindrical sheet of the mold in order to suppress a reaction between molybdenum sheet and the molten nickel as insulated ceramics and also to maintain the moisture. Figure 3.45 shows the optical micrographs of lotus nickel in parallel section to the solidification direction. The moisture contents in the mold weigh (a) 0.0596 g, (b) 0.0876 g, (c) 0.1070 g, and (d) 0.1201 g. In the ingot with the smallest amount of

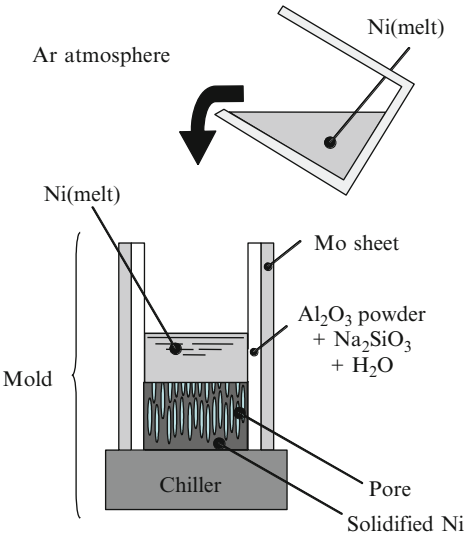

Fig. 3.44 Schematic drawing of the process of mold casting technique for fabrication of lotus nickel with moisture in argon atmosphere (Reprinted with permission from [42]. © 2004 Japan Institute of Metals)

moisture, almost all pores are spherical and long-cylindrical pores were not observed. The number of elongated pores increases with increasing moisture. Such longer pore evolution may be attributed to increase in hydrogen content which serves as a source for pore growth.

Figure 3.46 shows the magnified optical micrographs of cross-sectional planes (a) parallel and (b) perpendicular to the solidification direction at 4.5 mm in height from the bottom of the ingot (c) in Fig. 3.45, whose porosity is 44.7 % and the average pore size is 105 μm, ranging from 5 to 200 μm in diameter. On the other hand, for example, the porosity and pore size are 49.8 % and 499 μm, respectively, in lotus nickel fabricated using the dried mold without moisture under the pressure of 0.6 MPa argon and 0.2 MPa hydrogen. Thus, the porosity in lotus nickel fabricated in the mold with moisture in argon is as high as that in lotus nickel without moisture in hydrogen, and moreover, the pores can be more minute than that using hydrogen.

The pore evolution model by moisture was proposed by Suematsu et al. [42]. Figure 3.47 illustrates schematic of pore evolution process before solidification, after pouring the melt and during solidification. The moisture is absorbed in the ceramic coat on the lateral side of the mold, and then, when the molten nickel is poured into the mold, the moisture is dissolved into hydrogen and oxygen as a result of chemical reaction between the molten metal and moisture:

$$n\ H_2O(\text{gas}) + m\ M \leftrightarrow M_mO_n + 2n\ H, \tag{3.9}$$

where M is a metallic element to be oxidized easily. Then, the hydrogen is absorbed in the molten nickel and insoluble hydrogen when nickel is solidified is

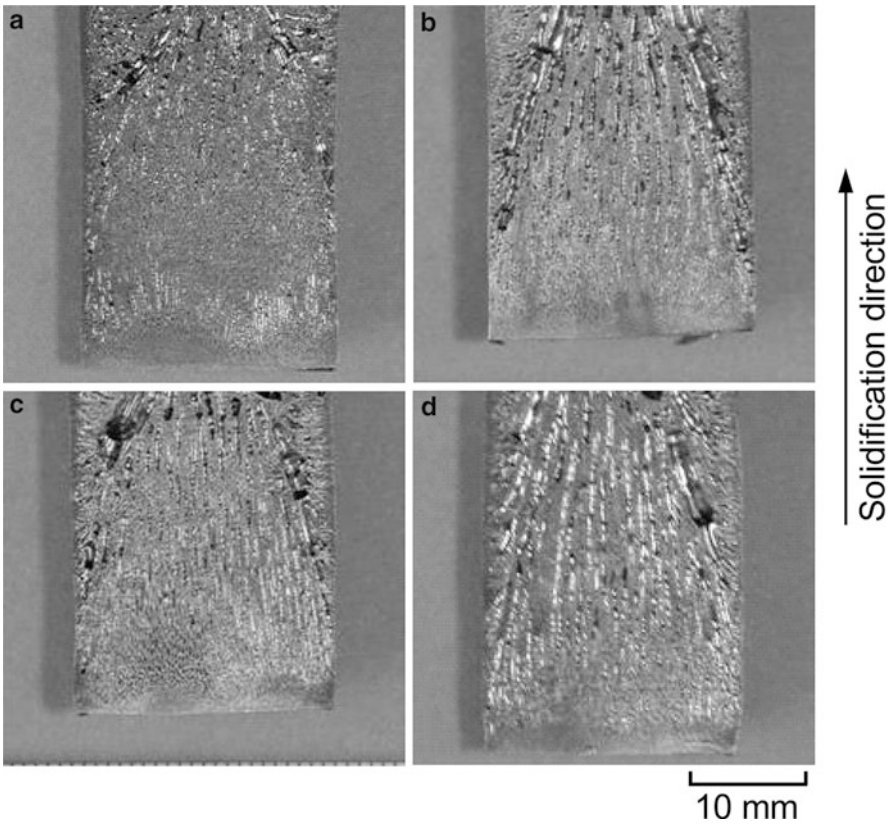

Fig. 3.45 Optical micrographs of lotus nickel in parallel section to the solidification direction (argon pressure, 0.3 MPa); moisture contents in mold are (**a**) 0.0596 g, (**b**) 0.0876 g, (**c**) 0.1070 g, and (**d**) 0.1201 g (Reprinted with permission from [42]. © 2004 Japan Institute of Metals)

able to form pores, whose principle is the same as that in fabrication of lotus metals. On the other hand, oxygen forms oxides with, for example, nickel which may become to be heterogeneous nucleation sites. It is well known that the pore nucleation takes place by heterogeneous nucleation mechanism. Thus, dissolution of oxygen in the melt increases the number of the pore nucleation sites. Even if the same amount of hydrogen dissolves in the molten nickel, a number of more minute elongated pores can be evolved using the mold with sufficient moisture in comparison with that using the dry mold in hydrogen atmosphere. Therefore, lotus-type porous nickel with minute elongated gas pores can be successfully produced by using the mold with moisture, which is far easy and simple technique to fabricate lotus metals.

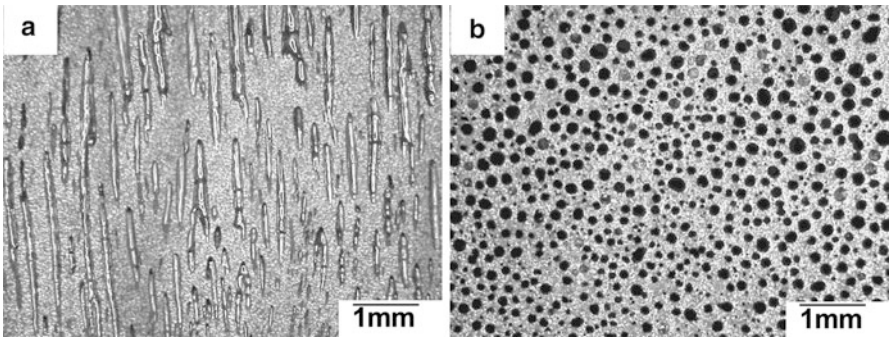

Fig. 3.46 Optical micrographs of cross sections of lotus nickel with 44.7 % porosity (argon pressure, 0.3 MPa). The cross-sectional plane (**a**) parallel and (**b**) perpendicular to solidification direction at 4.5 mm from the bottom plane in the ingot (Reprinted with permission from [42]. © 2004 Japan Institute of Metals)

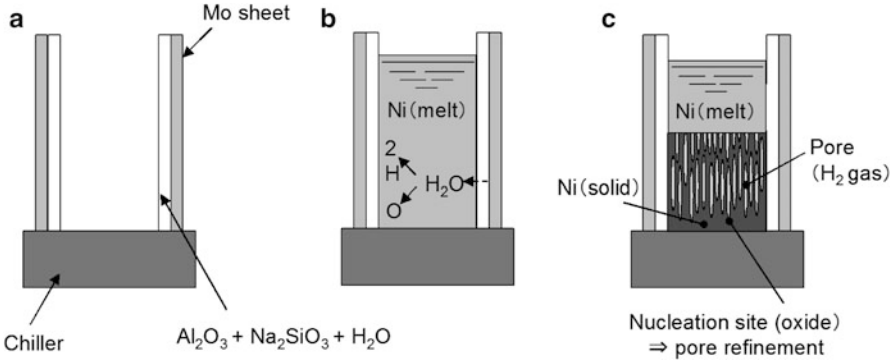

Fig. 3.47 Schematic drawings of pore-forming process. (**a**) Mold assembly before solidification, (**b**) molten nickel in the mold just after pouring of the melt, and (**c**) process of unidirectional solidification (Reprinted with permission from [42]. © 2004 Japan Institute of Metals)

3.4.2 Fabrication of Lotus Cobalt and Silicon by Moisture

Previous study as described in Sect. 3.4.1 suggests that formation of pores strongly depends on the dissociation constant of water at the casting temperature [42]. Because the free energy changes of Eq. (3.9) are known to be positive values, the dissociation constant P_{H_2}/P_{H_2O} is very small [43, 44]. It is worthwhile to investigate in detail whether the feasibility of pore formation on other materials is also closely related with the magnitude of the dissociation constant of water in the moist atmosphere. The feasibility to fabricate lotus silicon, cobalt, and copper was investigated by unidirectional solidification using moisture contained in the mold [45].

The metal in the crucible was melted by an induction coil and the melted metal was poured into the mold. The bottom of the mold was cooled by a water chiller, while the lateral wall was made of molybdenum whose surface was coated with a mixture of alumina, water glass (54.5 % H_2O, 31.2 % SiO_2, and 14.3 % Na_2O), and water with a weight ratio of 1:1.5:1. The mold was dried in an oven at 423 K for 7.2 ks. Then, the mold was kept in a closed chamber with constant humidity (90 %), which was measured by a hydrometer attached to the chamber for a given time, and 0.15 g of water, which corresponds to 0.083 mol of H_2O, was reabsorbed into the coating material. This value is sufficient to produce pores. About 2 mol of silicon, cobalt, and copper ingots with 99.9 % purity were used for casting. The size of the solidified ingots was 28 mm in diameter and 50 mm in length.

Figure 3.48 shows the cross-sectional views of solidified ingots of Si, Co, and Cu perpendicular and parallel to the solidification direction under a given pressure of the argon atmosphere. The pores elongated along the solidification direction were observed for Si and Co, while no pores were observed for Cu. Moreover, lotus Si and Co were also fabricated in the hydrogen atmosphere in the mold without moisture. The pore size in the lotus Si and Co fabricated in hydrogen gas is much larger than that by moisture dissociation, as shown in Fig. 3.49. When the moisture contained in the oxides mixture coated on the molybdenum mold was completely removed by drying, only nonporous cobalt ingot was obtained so that the pore evolution is attributed to hydrogen decomposed from the moisture in the mold. According to the previous investigation [10], lotus copper was easily produced by unidirectional solidification in pressurized hydrogen atmosphere. However, lotus copper was not produced by the moisture in the mold. In order to elucidate the reason why the moisture can produce lotus cobalt and silicon, not lotus copper, the ratio of pressure of hydrogen decomposed to that of the moisture was evaluated to the following reactions:

$$\mathrm{Co} + \mathrm{H_2O} = \mathrm{CoO} + \mathrm{H_2}, \tag{3.10}$$

$$\mathrm{Si} + 2\mathrm{H_2O} = \mathrm{SiO_2} + 2\mathrm{H_2}. \tag{3.11}$$

They assume that the moisture on the mold decomposes to hydrogen and oxygen atoms at the initial stage of casting. According to the Ellingham diagram, the ratio of hydrogen to moisture, P_{H_2}/P_{H_2O}, can be derived from the Gibbs free energy changes [43, 44]. Figure 3.50 shows the formation free energy changes of water and nickel, silicon, cobalt, and copper oxides. Porous nickel was fabricated by the mold casting method ratio of P_{H_2}/P_{H_2O}, at the casting temperature was approximately 1.18×10^{-2}, as calculated using the following equation:

$$\frac{P_{\mathrm{H_2}}}{P_{\mathrm{H_2O}}} = \exp\left(-\frac{\Delta G}{2RT}\right), \tag{3.12}$$

where ΔG, R, and T denote the Gibbs free energy change, the gas constant, and the casting temperature, respectively. The ratio of P_{H_2}/P_{H_2O}, for the formation of

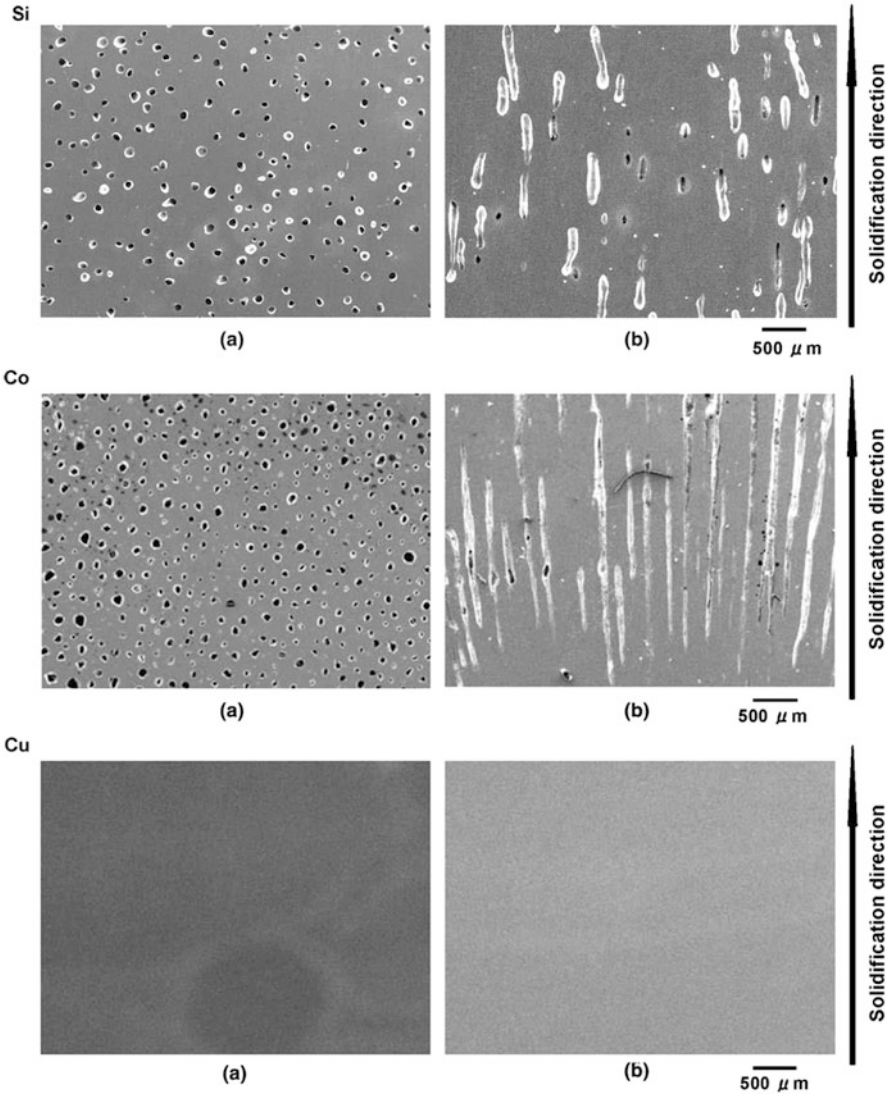

Fig. 3.48 (**a**) Transverse cross-sectional and (**b**) longitudinal cross-sectional views of lotus silicon, cobalt, and copper fabricated under Ar pressure. Argon pressure for each fabrication is 0.4 MPa for Si, 0.8 MPa for Co, and 0.4 MPa for Cu (Reprinted with permission from [45]. © 2008 The Minerals, Metals & Materials Society and ASM International)

silicon, cobalt, and copper oxides, is estimated as 2.15×10^4 at 1,773 K, 6.93×10^{-2} at 1,873 K, and 4.91×10^{-4} at 1,673 K, respectively [43, 44], as shown in Table 3.3. Assuming that the initial stage of casting is in the equilibrium state, the amount of moisture decomposed into hydrogen and oxygen atoms and the amount of hydrogen gas dissolved into the molten metal can be evaluated by the

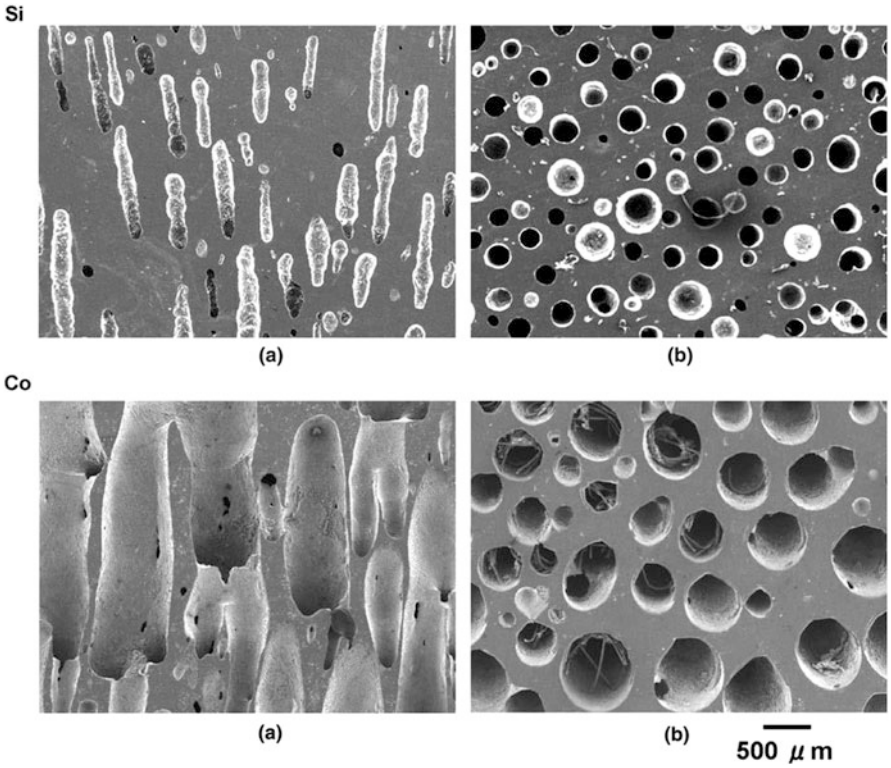

Fig. 3.49 (**a**) Longitudinal cross-sectional and (**b**) transverse cross-sectional views of lotus silicon fabricated under hydrogen pressure of 0.4 MPa and cobalt fabricated under hydrogen pressure of 0.15 MPa and argon pressure of 0.65 MPa (Reprinted with permission from [45]. © 2008 The Minerals, Metals & Materials Society and ASM International)

ratio of P_{H_2}/P_{H_2O} and the Sieverts law. The formation mechanism of the moisture decomposition into the molten metal is essentially the same as that of the method using pressurized hydrogen gas. These results indicate that the pores can be evolved, even if the value of P_{H_2}/P_{H_2O} is very small. Since no hydrogen gas was introduced in the chamber, the hydrogen partial pressure in the atmosphere is considered as 0 MPa. Hence, the hydrogen gas used in the formation of pores is formed by decomposition of the moisture on the mold during solidification.

The pore diameter for the lotus silicon and cobalt fabricated in the moisture method is much smaller than that of those fabricated under pressurized hydrogen atmosphere. It is well known that heterogeneous nucleation takes place in metal melts in the presence of small amounts of foreign elements [34]. Then, it is reasonable to consider that oxygen decomposed from the moisture can result with a metallic element to form oxide clusters, which are nuclei for pore evolution as illustrated in Fig. 3.51. Such dispersive oxide clusters may promote uniform small

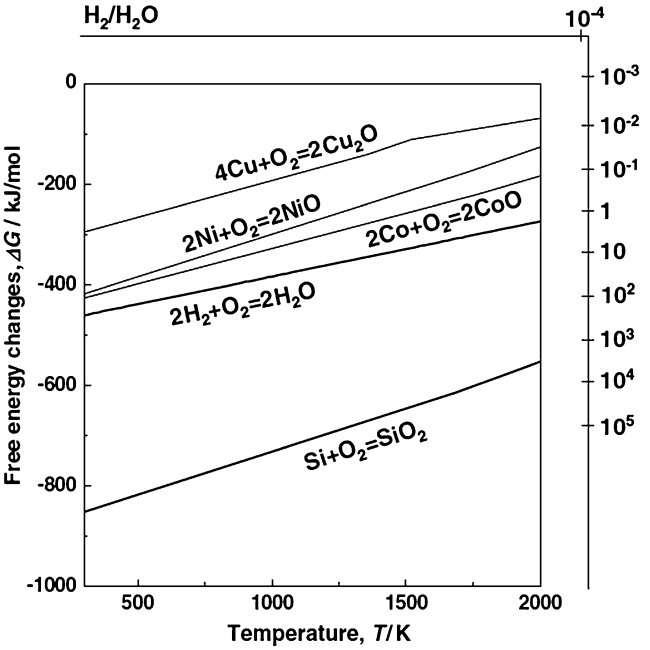

Fig. 3.50 Temperature dependence of the change of the free energy for formation of water, silica, cobalt oxide, nickel oxide, and copper oxide [43, 44] (Reprinted with permission from [45]. © 2008 The Minerals, Metals & Materials Society and ASM International)

Table 3.3 Free energy changes of dissociation of water for Si, Co, Cu, and Ni

R reaction	ΔG (kJ mol^{-1})	Casting temperature (K)	P_{H_2}/P_{H_2O}
$Si + 2H_2O = SiO_2 + 2H_2$	−298.5	1,773	2.15×10^{4}
$Co + H_2O = CoO + H_2$	41.56	1,873	6.93×10^{-2}
$2Cu + H_2O = Cu_2O + H_2$	53.41	1,673	4.91×10^{-4}
$Ni + H_2O = NiO + H_2$	69.13	–	1.18×10^{-2}

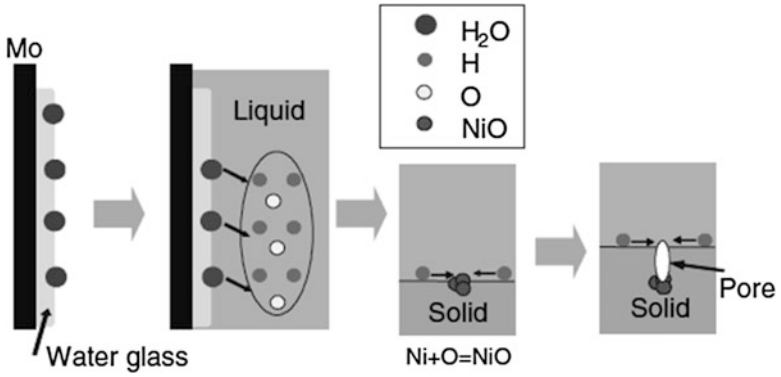

Fig. 3.51 Schematic growing of the movement of oxide during fabrication and pore generation (Reprinted with permission from [45]. © 2008 The Minerals, Metals & Materials Society and ASM International)

pore distribution. Although quantitative comparison of the moisture decomposition method with the pressurized hydrogen method is not possible, there is a tendency that the moisture method can produce smaller-sized pores and a large number of density of pores. This tendency can be explained in terms of the oxide clusters for possible nucleation sites.

References

1. Chalmers B (1959) Sci Am 200:114–122
2. Imabayashi M, Ichimura M, Kanno Y (1983) Trans JIM 24:93–100
3. Svensson I, Fredriksson HS (1980). In: Proceedings of international conference organized by the applied metallurgy and metals tech group of TMS, University of Warwick, pp. 376–380
4. Knacke O, Probst H, Wernekinck J (1979) Z Metallkde 70:1–6
5. Bioko LV, Shapovalov VL, Chernykh EA (1991) Metallurgiya 346:78–81
6. Hyun SK, Shiota Y, Murakami K, Nakajima H (1999) In: Koiwa M, Otsuka K, Miyazaki T (eds) Proceedings of international conference on solid-solid phase transformations '99 (JIMIC-3), Japan Inst Metals, Kyoto, pp. 341–344
7. Nakajima H, Hyun SK, Ohashi K, Ota K, Murakami K (2001) Colloids Surf A:Physicochem Eng Aspects 197:209–214
8. Nakajima H (2001) Mater Trans 42:1827–1829
9. Shapovalov VI (1994) MRS Bull XIX:24–28
10. Hyun SK, Murakami K, Nakajima H (2001) Mater Sci Eng A 299:241–248
11. Smith DP (1947) Hydrogen in metals. The University of Chicago Press, Chicago, p 34
12. Reed-Hill RE (1964) Physical metallurgy principles. D.Van Nostrand Company Inc, Princeton, p 393
13. Massalski TB (1986) Binary alloy phase diagram. American Society for Metals, Metals Park, p 1079
14. Levinsky Y (1997) Pressure dependent phase diagrams of binary alloys. ASM International, Materials Park, p.693
15. Satir-Kolorz AH, Feichtinger HK (1991) Z Metallkde 82:689–697
16. Hyun SK, Nakajima H (2002) Mater Trans 43:526–531
17. Nakahata T, Nakajima H (2005) Mater Trans 46:587–592
18. Ikeda T, Nakajima H (2002) Japan Foundry Eng Soc 74:812–816
19. Hyun SK, Nakajima H (2003) Mater Lett 57:3149–3154
20. Ikeda T, Tsukamoto M, Nakajima H (2002) Mater Trans 43:2678–2684
21. Nakajima H, Ikeda T, Hyun SK (2003) In: Banhart J, Fleck A (eds) Cellular metals: manufacture, properties, applications. MIT, Berlin, pp 191–202
22. Nakajima H, Ikeda T, Hyun CK (2004) Adv Eng Mater 6:377–384
23. Ikeda T, Aoki T, Nakajima H (2005) Metall Mater Trans A 36A:77–86
24. Park JS, Hyun SK, Suzuki S, Nakajima H (2007) Acta Mater 55:5646–5654
25. Campbell J (1991) Castings. Butterworth-Heinemann, Oxford
26. Fisher JC (1948) J Appl Phys 19:1062–1067
27. Flemings MC (1974) Solidification processing. McGraw-Hill, New York
28. Chalmers B (1964) Principles of solidification. Wiley, New York
29. Porter DA, Easterling KE (1992) Phase transformations in metals and alloys. Chapman & Hall, London
30. Fromm E, Gebhardt E (1976) Gases and carbon in metals. Springer, Berlin
31. Wright JH, Hocking MG (1972) Metall Trans 3:1749–1753
32. Nakajima H, Ide T (2008) Metall Mater Trans A 39A:390–394

33. Nakajima H, Ide T (2007) Method for manufacturing porous body. PCT/JP2007/062769 (patent pending)
34. Fredriksson H, Akerlind U (2006) Materials processing during casting. Wiley, Chichester, pp 141–142
35. Kim SY, Park JS, Nakajima H (2009) Metall Mater Trans A 40A:937–942
36. Makaya A, Fredriksson H (2005) Mater Sci Eng A 413A–414A:533–537
37. Wada T, Ide T, Nakajima H (2009) Metall Mater Trans A 40A:3204–3209
38. Murray P, White J (1955) Trans Br Ceram Soc 54:204–237
39. Tiller WA, Jackson KA, Rutter JW, Chalmers B (1953) Acta Metall 1:428–437
40. Kissinger HE (1957) Anal Chem 29:1702–1706
41. Nakajima H, Ide T (2012) In: Proceedings of cellular materials (Cellmat2012), Deutsche Gesellschaft fur Materialskunde e.V, pp. 1–4
42. Suematsu T, Hyun SK, Nakajima H (2004) J Japan Inst Metals 68:257–261
43. Kubaschewski O, Alcock CB (1979) Metallurgical thermochemistry, 5th edn. Pergamon, Oxford
44. Elliott JF, Gleiser M, Ramakrishna V (1963) Thermochemistry for steelmaking, vol 1. Addition-Wesley, New York, pp 161–215
45. Onishi H, Ueno S, Hyun SK, Nakajima H (2009) Metall Mater Trans A 40A:438–443